

1 **Explosive felsic eruptions on ocean islands: a case study from Ascension**
2 **Island (South Atlantic)**

3
4 Katie Preece^{1*}, Jenni Barclay², Richard J. Brown³, Katy J. Chamberlain⁴, Darren F. Mark^{5,6}

5
6 1. Department of Geography, Faculty of Science and Engineering, Swansea University,
7 Singleton Park, Swansea, SA2 8PP, UK

8 2. School of Environmental Sciences, University of East Anglia, Norwich, NR4 7TJ, UK

9 3. Department of Earth Sciences, Durham University, Science Labs, Durham, DH1 3LE,
10 UK

11 4. Environmental Sciences Research Centre, University of Derby, Derby, DE22 1GB, UK

12 5. Scottish Universities Environmental Research Centre, Rankine Avenue, East Kilbride,
13 G75 0QF, UK

14 6. Department of Earth & Environmental Science, University of St Andrews, St Andrews,
15 KY16 9AJ, UK

16
17 * Corresponding Author

18 *Email Address:* k.j.preece@swansea.ac.uk

19
20 **Submitted to Journal of Volcanology and Geothermal Research**

23 **Abstract**

24 Ocean island volcanism is generally considered to be dominated by basaltic eruptions,
25 yet felsic products associated with more hazardous explosive eruptive events are also present
26 in the geological record of many of these islands. Ascension Island, recently recognised as an
27 active volcanic system, exhibits explosive felsic eruption deposits but their age, eruptive styles
28 and stratigraphic association with mafic volcanism are thus far unclear. Here we present a felsic
29 pyroclastic stratigraphy for Ascension Island, supplemented by 26 new $^{40}\text{Ar}/^{39}\text{Ar}$ ages and
30 whole rock geochemical XRF data. More than 80 felsic pyroclastic eruptions have occurred
31 over the last ~ 1 Myr, including subplinian and phreatomagmatic eruptions, which produced
32 pumice fall and pyroclastic density current deposits. Detailed sampling suggests felsic events
33 are unevenly distributed in space and time. Subaerial activity can be divided into four Periods:
34 Period 1 (~1000 – 500 ka) felsic and mafic eruptions, with felsic explosive eruptions, linked to
35 a Central Felsic Complex; Period 2 (~ 500 – 100 ka) mafic period; Period 3 (~ 100 – 50 ka)
36 felsic eruptions associated with the Eastern Felsic Complex; Period 4 (< 50 ka) mafic eruptions.
37 The last explosive eruption occurred at ~ 60 ka. This work highlights the cyclical nature of
38 ocean island volcanism and the timescales over which changes between predominantly mafic
39 and felsic volcanism occur. The prevalence of past felsic explosive eruptions on Ascension
40 highlights the need to consider the possibility of future subplinian or phreatomagmatic events
41 in hazard management plans, with any potential risk compounded by Ascension's small size
42 and remote location.

43

44 **Keywords:** Ascension Island, pyroclastic eruption, volcanic stratigraphy, $^{40}\text{Ar}/^{39}\text{Ar}$
45 geochronology, volcanic hazards

46

47 **1.0 Introduction**

48 Ocean island volcanoes are predominantly associated with basaltic magma
49 compositions, producing lava flows and mildly-explosive scoria cones. However, felsic
50 deposits are also present in ocean island geological records, albeit to varying degrees. For
51 example, even dominantly basaltic volcanic islands such as Hawaii and Iceland have produced
52 evolved rocks, and deposits associated with explosive felsic activity (*e.g.* Cousens et al., 2003;
53 Jónasson, 2007; Shea and Owen, 2016). Peralkaline trachytes and rhyolites constitute ~ 80 %
54 of the surface exposure of Socorro Island (Mexico), including deposits linked to caldera
55 formation (Bohrson and Reid, 1997), and peralkaline phonolites make up ~ 65 % of the surface
56 of Ua Pou Island (Marquesas, French Polynesia) (Legendre et al., 2005). Within the Atlantic,
57 extensive felsic deposits have been described on the Canary Islands, with the greatest
58 abundance of felsic rocks on the islands of Gran Canaria and Tenerife, where felsic pyroclastic
59 density current (PDC) and pumice fall deposits are widespread (*e.g.* van den Bogaard, 1998;
60 Kobberger and Schmincke, 1999; Brown and Branney, 2004). In the Azores, felsic magmas
61 have erupted from central volcanoes mostly via subplinian events, as well as lava domes and
62 coulées, in particular on the islands of São Miguel, Terceira and Faial (*e.g.* Guest et al., 1999;
63 Queiroz et al., 2008; Gertisser et al., 2010; Pimentel et al., 2015). The Cape Verde islands are
64 composed of a range of rock types, but the subaerial geology of Brava Island is dominated by
65 phonolitic pyroclastic products, lava domes and lava flows (*e.g.* Madeira et al., 2010). Felsic
66 magmas can erupt effusively or explosively, generating multiple hazards. Importantly,
67 explosive felsic eruptions may pose elevated risk to volcanic islands, due to their small size,
68 geographic remoteness and lack of systems for early-warning and hazard management (*e.g.*
69 Komorowski et al., 2016; Wilkinson et al., 2016; Selva et al., 2019). Reconstructing volcanic
70 histories, including understanding the character and timing of previous eruptions, is essential

71 for anticipating likely impacts of future eruptions and for generating long-term hazard
72 assessments (*e.g.* Marzocchi and Bebbington, 2012).

73 Ascension Island (7°56'S, 14°22'W) is a small (98 km²) ocean island volcano, located
74 ~ 90 km west of the Mid-Atlantic Ridge. The island is a British Overseas Territory, with a
75 population of ~ 800. The active nature of the island has only recently been revealed, with the
76 last eruption occurring at 0.51 ± 0.18 ka, which produced mafic lava flows and scoria (Preece
77 et al., 2018). Felsic pyroclastic deposits have been noted on Ascension (*e.g.* Nielson and
78 Sibbett, 1996; Kar et al., 1998; Hobson, 2001), and it has been estimated that trachytic and
79 rhyolitic products form 14 % of the surface exposure of the island (Nielson and Sibbett, 1996),
80 with pyroclastic material (pumice and scoria) covering 43 % of the island's surface (Harris et
81 al., 1983). However, the felsic pyroclastic deposits have not been described in detail, and little
82 is known about their age.

83 In considering Ascension's active volcanic status, small size and isolated nature, it is
84 crucial to gain an understanding of the explosive eruptive history of the island, to better inform
85 hazard assessment. Here we present the first detailed stratigraphy and ⁴⁰Ar/³⁹Ar geochronology
86 of the felsic pyroclastic deposits on Ascension Island. Results show that felsic explosive
87 eruptions have been common during the last 1 Myr, and produced a variety of volcanic hazards.
88 These findings contribute an important insight into the nature and periodicity of felsic
89 pyroclastic eruptions in an ocean island setting. Results create a crucial framework for the
90 anticipation of future hazard and understanding the long-term evolution of the magmatic
91 plumbing system.

92

93 **2. 0 Background**

94 ***2.1 Geological Setting***

95 Most previous geological work on Ascension has focused on understanding tectonic
96 association, petrogenesis, and magmatic processes, using geophysical, geochemical and
97 petrological techniques (*e.g.* Weaver et al., 1996; Kar et al., 1998; Klingelhöfer et al., 2001;
98 Paulick et al., 2010; Chamberlain et al., 2016, 2019, 2020). Ascension is located on 5 – 7 Ma
99 oceanic crust (Klingelhöfer et al., 2001; Paulick et al., 2010), situated between the Ascension
100 and Bode Verde fracture zones (Fig. 1). Whilst some studies have linked Ascension with a
101 mantle plume source (*e.g.* Brozena, 1986; Montelli et al., 2006), other geophysical work
102 revealed a crustal structure beneath Ascension which is inconsistent with a hotspot, and a lack
103 of magmatic underplating, instead suggesting an on-axis origin (Klingelhöfer et al., 2001;
104 Evangelidis et al., 2004). Isotopic data point to on-axis growth of the submarine volcanic
105 edifice, with subsequent volcanism continuing off-axis with partial melting of an enriched
106 mantle source producing the subaerial portion of the island (Paulick et al., 2010).

107 Early descriptions of the general geology of Ascension are given in Daly (1925), Atkins
108 et al. (1964) and Nielson and Sibbett (1996). Ascension shows a large diversity of erupted
109 products, in terms of both geochemical composition and eruptive style, including voluminous
110 production of felsic magma which has erupted both effusively and explosively. Ascension
111 volcanic products typically define a transitional to mildly alkaline basalt-hawaiite-mugearite-
112 benmoreite-trachyte-rhyolite series, where $(\text{Na}_2\text{O} - 2) > \text{K}_2\text{O}$ (Weaver *et al.*, 1996), with the
113 more evolved compositions having a peralkaline character (Jeffery and Gertisser, 2018)
114 (Peralkalinity Index = molar $(\text{Na}_2\text{O} + \text{K}_2\text{O})/\text{Al}_2\text{O}_3 > 1$). The northern, western and southern
115 portions of the island comprise scoria cones and mafic lava flows (Fig. 1), previously
116 subdivided into three groups on the basis of Zr/Nb (Low, Intermediate and High Zr/Nb)
117 (Weaver et al., 1996). The central and eastern areas of the island are mainly composed of
118 trachyte and rhyolite lava flows, domes and pyroclastic material. The occurrence of felsic rocks
119 on an ocean island volcano received attention from Charles Darwin when he visited Ascension

120 in 1836 as part of the Beagle Voyage (Darwin, 1844). At Ascension, felsic compositions are
121 thought to form via fractional crystallisation from alkali basalt, without magma mixing or
122 crustal assimilation (Weaver et al., 1996; Kar et al., 1998; Jicha et al., 2013; Chamberlain et
123 al., 2016, 2019), and there is evidence that some of these evolved melts were produced and
124 stored within the lower crust (Chamberlain et al., 2020). The felsic products are related to a
125 Central Felsic Complex and an Eastern Felsic Complex (*e.g.* Kar et al., 1998) (Fig. 1).

126

127 **2.2 Volcanic history and geochronology**

128 $^{40}\text{Ar}/^{39}\text{Ar}$ geochronology of lavas from a borehole on Ascension, indicates that the shift
129 from submarine to subaerial eruptions occurred at ~ 2.5 Ma (Minshull et al., 2010). However,
130 the oldest dated subaerial deposit exposed at the surface on Ascension is a rhyolite lava flow
131 at Middleton Ridge, which has been dated by the $^{40}\text{Ar}/^{39}\text{Ar}$ technique at 1094 ± 12 ka (Jicha et
132 al., 2013). A trachyte lava was dated at 1.5 ± 0.2 Ma using the K-Ar technique (Harris et al.,
133 1982), although this age has been questioned by Nielson and Sibbett (1996) who re-dated the
134 lava to 0.6 ± 0.3 Ma, also using the K-Ar technique. The most recent eruptions produced
135 hawaiite and mugearite lava flows and scoria in the north and northwest of the island, dated by
136 the $^{40}\text{Ar}/^{39}\text{Ar}$ technique at 0.51 ± 0.18 ka, 0.55 ± 0.12 ka and 1.64 ± 0.37 ka (Preece et al.,
137 2018). The subaerial eruptive chronology has previously relied strongly on the $^{40}\text{Ar}/^{39}\text{Ar}$ dating
138 of lavas and has been divided into five stages: 1) 1094 – 719 ka: comprising Middleton Ridge
139 trachyte and rhyolite lavas; 2) 829 – 652 ka: trachyte situated north and west of Middleton
140 Ridge and mafic lavas; 3) 637 – 602 ka: trachyte domes and flows on the southwest slope of
141 Green Mountain; 4) 589 – 298 ka: mafic volcanism mainly concentrated in the southern half
142 of the island; 5) < 169 ka: Eastern Felsic Complex and Holocene mafic eruptions (Jicha et al.,
143 2013).

144 Based on field observations and limited dating, Kar et al., (1998) proposed that the
145 Eastern Felsic Complex was probably younger than the Central Felsic Complex. This is in
146 agreement with the stages of Jicha et al., (2013) who dated felsic lava in the Eastern Felsic
147 Complex as young as 52 ± 3 ka. Until now, the pyroclastic products have received little
148 attention. An initial pyroclastic stratigraphy was defined during the course of a palaeomagnetic
149 investigation, which identified five major pyroclastic eruptions (Lower Pumice, Middle
150 Pumice, Upper Pumice 1, 2 and 3) (Hobson, 2001), and only one pumice unit has previously
151 been dated (Kar *et al.*, 1998). In order to aid hazard analysis and long-term contingency
152 planning, it is crucial that the full range of eruptive styles on Ascension are understood, and
153 that the timing of explosive eruptions is constrained.

154

155 **3.0 Methods**

156 ***3.1 Field data and stratigraphy***

157 During field stratigraphic analysis, lithostratigraphic units were defined based upon
158 observable and distinctive lithological properties (lithofacies) and stratigraphic relations
159 (Murphy and Salvador, 1999; Luchhi et al., 2010; Lucchi, 2013). The lithofacies descriptions
160 and abbreviations are listed in Table 1. Eruption units may be defined as volcanic material
161 emplaced during a single eruptive pulse (activity lasting seconds to minutes), eruptive phase
162 (hours to days) or single eruption that may have lasted days to months and is often composed
163 of multiple eruptive pulses (Fisher and Schmincke, 1984). Single eruption units are key to this
164 study, in order to gain an understanding of the eruptive history in terms of number, style and
165 size of explosive felsic eruptions. On Ascension, many lithostratigraphic units are bounded by
166 unconformities and evidence of hiatuses, in the form of erosion surfaces, angular
167 unconformities, deposition of reworked material, and/or weathering of palaeo-surfaces

168 evidenced by the discoloration of primary clasts. Palaeosols are not common on Ascension.
169 Thus, eruption units have been defined based upon interpretation of observed lithostratigraphic
170 units, coupled with evidence for depositional time gaps. Eruption units found on Ascension
171 include pyroclastic fall units, pyroclastic density current units, and lava flow units, depending
172 upon the interpreted manner of emplacement. Many lithostratigraphic units on Ascension are
173 not traceable or possible to correlate between exposures due to poor preservation, with many
174 units only outcropping in one locality.

175

176 **3.2 $^{40}\text{Ar}/^{39}\text{Ar}$ geochronology**

177 $^{40}\text{Ar}/^{39}\text{Ar}$ ages were obtained from feldspar phenocrysts. Feldspar phenocrysts in
178 Ascension pumice are mainly oligoclase to anorthoclase \pm sanidine. The least evolved sample
179 in this study (Middleton Fall; AI14-459A) contained oligoclase to andesine plagioclase (see
180 Chamberlain et al. (2019) for representative feldspar compositions). Feldspar phenocrysts were
181 separated from fresh juvenile pumice and scoria using the methods of Mark et al. (2017).
182 Briefly, pyroclasts were crushed in a jaw crusher, sieved, washed repeatedly in de-ionized
183 water, before the $> 500 - < 710 \mu\text{m}$ size fractions were magnetically separated to isolate
184 feldspar phenocrysts. The feldspar phenocrysts were leached in an ultrasonic bath in 5% HF
185 for 5 minutes to remove adhering groundmass glass, before being rinsed three times in de-
186 ionized water in an ultrasonic bath. Once dried, the feldspars were passed through a magnetic
187 separator at low speed and low angle of tilt, to remove feldspar phenocrysts with mineral or
188 melt inclusions. Samples were then hand-picked under a binocular microscope to eliminate any
189 remaining crystals containing inclusions and any visibly altered crystals. Pristine crystals were
190 parcelled into Cu packets, or Al discs, stacked in glass vials and sealed in a large glass vial for
191 irradiation. International standard Alder Creek sanidines (ACs; with an age of 1.1891 ± 0.0008
192 Ma; Niespolo et al., 2017) were used as fluence monitors for J-determination and packaged

193 throughout the stack at known spacing (geometry) in between samples. Samples and standards
194 were irradiated in 3 different batches at the Cd-lined (CLICIT) facility of the Oregon State
195 University (USA) TRIGA reactor, all for 2 hours. J-measurements were obtained using either
196 a MAP 215-50 noble gas mass spectrometer (Mark et al., 2014) or a HELIX-SFT multicollector
197 noble gas mass spectrometer (Pickersgill et al., 2020). Single irradiated crystals ($n= 30$ per
198 sample) were fused with a CO₂ laser and isotope data were collected using the either a MAP
199 215-50 noble gas mass spectrometer or a HELIX-SFT multicollector noble gas mass
200 spectrometer that has custom modifications for ⁴⁰Ar/³⁹Ar geochronology (Mark et al., 2009).

201 Samples were analyzed in several batches; backgrounds and mass discrimination
202 measurements (via automated analysis of multiple air pipettes) specific to each batch were used
203 to correct the data. Air pipettes were run (on average) after every 4 analyses. Backgrounds
204 subtracted from ion beam measurements were arithmetic averages and standard deviations.
205 Mass discrimination was computed based on a power law relationship (Renne et al., 2009)
206 using the isotopic composition of atmospheric Ar reported (Lee et al., 2006) that has been
207 independently confirmed (Mark et al., 2011). Corrections for radioactive decay of ³⁹Ar and
208 ³⁷Ar were made using the decay constants reported by Stoenner et al. (1965) and Renne and
209 Norman (2001), respectively. Ingrowth of ³⁶Ar from decay of ³⁶Cl was corrected using the
210 ³⁶Cl/³⁸Cl production ratio and methods of Renne et al. (2008) and was determined to be
211 negligible. Argon isotope data corrected for backgrounds, mass discrimination, and radioactive
212 decay and ingrowth are given in Supplementary Material 1. Data plots are shown in
213 Supplementary Material 2.

214 The samples were analyzed by total fusion and step-heating with a CO₂ laser. The mass
215 spectrometers are both equipped with Nier-type ion sources. The MAP 215-50 data was
216 collected using an analogue electron multiplier detector. The HELIX-SFT utilized a
217 combination of detectors; ⁴⁰Ar was measured using a Faraday cup equipped with a 10¹² Ohm

218 amplifier and ^{39}Ar - ^{36}Ar was measured using an ion counting electron multiplier. Mass
219 spectrometry in both cases utilized peak-hopping by magnetic field switching for 10 cycles.

220 Ages were computed from the blank-, discrimination- and decay-corrected Ar isotope
221 data after correction for interfering isotopes based on the following production ratios,
222 determined from fluorite and Fe-doped KAlSiO_4 glass: $(^{36}\text{Ar}/^{37}\text{Ar})_{\text{Ca}} = (2.650 \pm 0.022) \times 10^{-4}$;
223 $(^{38}\text{Ar}/^{37}\text{Ar})_{\text{Ca}} = (1.96 \pm 0.08) \times 10^{-5}$; $(^{39}\text{Ar}/^{37}\text{Ar})_{\text{Ca}} = (6.95 \pm 0.09) \times 10^{-4}$; $(^{40}\text{Ar}/^{39}\text{Ar})_{\text{K}} = (7.3 \pm$
224 $0.9) \times 10^{-4}$; $(^{38}\text{Ar}/^{39}\text{Ar})_{\text{K}} = (1.215 \pm 0.003) \times 10^{-2}$; $(^{37}\text{Ar}/^{39}\text{Ar})_{\text{K}} = (2.24 \pm 0.16) \times 10^{-4}$, as
225 determined previously for this reactor in the same irradiation conditions (Renne, 2014). Ages
226 and their uncertainties are based on the methods of Renne et al. (2010), the calibration of the
227 decay constant as reported by Renne et al. (2011) and the ACs optimization age ($1.1891 \pm$
228 0.0009 Ma, 1 sigma) as reported by Niespolo et al. (2017).

229 Outliers in both single-crystal samples and standards were discriminated using a 3-
230 sigma filter applied iteratively until all samples counted are within 3 standard deviations of the
231 weighted mean \pm one standard error. This procedure screened older crystals that are logically
232 interpreted as xenocrysts. No younger outliers were recorded during analysis of all samples.
233 Processing of the data using the *n*MAD approach of Kuiper et al. (2008) has no impact on the
234 probability distribution plots for each sample.

235 Both the probability spectra and the inverse isochron ages are reported (Table 2), and
236 are indistinguishable from each other. However, for consistency the ages reported in text and
237 figures are probability spectra ages, except in a few samples where the $^{40}\text{Ar}/^{36}\text{Ar}$ is
238 distinguishable from an atmospheric $^{40}\text{Ar}/^{36}\text{Ar}$ value of 298.56 ± 0.31 (Lee et al., 2006). In
239 these cases, the inverse isochron age is preferred (Table 2 and Supplementary Materials 1 and
240 2)

241

242 **3.3 Whole rock major and trace element XRF**

243 Whole rock pumice compositions were obtained from interior portions of fresh
244 samples, which were washed in Milli-Q water in a sonic bath, dried overnight at > 100°C and
245 powdered in a tungsten carbide mill, before fused glass discs and pressed powder pellets were
246 prepared for major and trace element analysis respectively. X-ray fluorescence (XRF) analysis
247 was carried out using a Bruker AXS S4 Pioneer at the University of East Anglia. Loss on
248 ignition (LOI) was carried out by heating ~ 1 g of sample powder in a furnace at 1050°C for 4
249 hours.

250

251 **4.0 Results**

252 Pyroclastic lithologies on Ascension Island are wide-ranging and numerous. Pumice
253 lapilli are abundant, and eruption units may be massive (mpL), stratified (spL) and often
254 containing ashy layers. The pumice is often only moderately sorted and sometimes displays
255 bimodal clast sizes due to the proximal nature of the units. The thickness of individual eruption
256 units of pumice lapilli range from < 1m, up to tens of metres thick. Pumice lapilli units are
257 interpreted to have formed via pumice fallout during explosive eruptions. Several massive
258 pumice breccia (mpBr) deposits are present, which contain pumice clasts up to > 10 cm in
259 diameter, with unit thicknesses generally ~ 2 – 3 m. These massive pumice breccias are
260 interpreted to be explosion breccias, deposited via pyroclastic fallout proximal to the vent.
261 Multiple massive tuffs (mT), and more commonly, massive lapilli tuffs (mLT) are present,
262 occasionally in association with eutaxitic lapilli tuffs (eLT), ranging in thickness from ~ 10 cm
263 to > 10 m. The mT units are interpreted to represent either ash fall or dilute, ash-rich pyroclastic
264 density current (PDC) deposits. The mLT deposits are interpreted to have formed via PDCs,
265 with lapilli componentry in the mLT units frequently pumice (ignimbrites), or composed of

266 scoria, probably formed from more mafic PDCs. Several massive lithic breccias (mlBr) occur,
267 which are ~ 1 – 5 m thick, interpreted to be explosion breccias, with no evidence of them being
268 linked to ignimbrite or pumice fall deposits. The felsic pyroclastic units are intercalated with
269 lavas and with scoria deposits. For example, scoria lapilli (mscL), scoria breccia (mscBr), and
270 scoria spatter agglomerate (mscAg) are situated in the stratigraphy between felsic pyroclastic
271 lithologies, and represent scoria fall deposits with varying proximity to the vent.

272 In the central region of the island, an abundance of pyroclastic deposits are exposed in
273 the vicinity of NASA Road, Middleton Ridge, Middleton Valley, within Devil’s Riding School,
274 and near the village of Two Boats (Fig. 1). Green Mountain is the highest peak (859 m) on
275 Ascension, located near the centre of island (Fig 1). Green Mountain is densely vegetated,
276 although the cuts on the road to the summit provide access to outcrops. Outcrops along the
277 entire length of the Green Mountain Road have been logged (Fig. 2). Here, multiple normal
278 faults dissect the exposures, sometimes displacing eruptive units to the extent that a continuous
279 stratigraphy is not possible to establish. In the east of the island, abundant felsic pyroclastic
280 units, in addition to felsic lava domes and lava flows are located in the region between Thistle
281 Hill and Upper Valley Crater, Goat Hole Ravine, Echo Canyon, in and around Cricket Valley,
282 near Devil’s Cauldron and Spire Beach (Fig. 1).

283 Based on the stratigraphy and the $^{40}\text{Ar}/^{39}\text{Ar}$ ages, we firstly sub-divide the observed
284 eruption units into those associated with three distinct time periods (1000 – 500 ka; 500 – 100
285 ka; < 100 ka) as described below.

286

287 ***4.1 1000 – 500 ka***

288 The deposits produced during this time period are predominantly preserved in the centre
289 of the island. The two oldest dated pyroclastic units in this study (Green Mountain Road 1 and

290 the Middleton Fall) are located within the central region of the island and have ages within
291 uncertainty of each other. The unit Green Mountain Road 1 ('GMR1') is located at the base of
292 the Green Mountain Road stratigraphy (Figs. 2 and 3a), dated at 916 ± 20 ka (AI14-551) (Fig.
293 4a,b), and is a trachytic pumice fall deposit, which is at least 7 m thick, although the base is not
294 exposed. The Middleton Fall (872 ± 81 ka; AI14-459A) is a pumice fall unit located in
295 Middleton Valley (Fig. 1). The Middleton Fall is > 3 m thick, with a mpL base, grading up to
296 become more scoria-rich in the top 1.3 m (Fig. 5 log 17). The benmoreite (Table 3) pumice
297 from the Middleton Fall deposit is notable as it is the least evolved pumice within this study
298 (62.2 wt.% SiO_2 when normalised to 100% on a volatile-free basis; Fig. 6) and it contains
299 phenocrysts of amphibole, the presence of which is rare on Ascension (Chamberlain et al.,
300 2019). Older deposits are present in the stratigraphy, below the Middleton Fall, however they
301 are very weathered and altered, thus were not dated (Fig. 5). Correlation between units in the
302 older portion of the stratigraphic record is not possible, as individual units are often only
303 present in one location and not traceable over wider areas, due to erosion and/or burial by more
304 recent deposits.

305 The deposit of a pumice-rich PDC (ignimbrite) ('NASA PDC') is located on Upper
306 NASA Road and in Middleton Valley, as well as on Green Mountain Road (Figs. 2 and 5). The
307 unit has not been directly dated, but on Upper NASA Road, it is situated stratigraphically
308 beneath a pumice breccia unit dated at 793 ± 8 ka (AI14-498F) (Figs. 4c,d and 5). On Upper
309 NASA Road, the ~ 2 m thick 'NASA PDC' unit is characterised by pumice fall (mpL) at the
310 base which grades into PDC deposit (mLT) (Fig. 7a), although only the PDC facies is present
311 in Middleton Valley and on Green Mountain Road. The ignimbrite facies is characterised by
312 its orange and white colour, elongated pumice at the base, and lithic clasts of lava, scoria and
313 plutonic cumulates. On Green Mountain Road, the unit is present in several locations, occurring
314 as an orange- and white-coloured massive lapilli tuff or eutaxitic massive lapilli tuff

315 (mLT/emLT) (Fig. 2). On Green Mountain Road, it ranges in thickness from 11 cm to ~ 2 m.
316 Here, the thickest occurrence is on the Residency Track (Fig. 3b), where the deposit displays
317 an erosive base, and contains pumice fiamme. In other localities on Green Mountain Road, the
318 deposit displays a eutaxitic texture, and a jointed top, representing cooling fractures. Another
319 notable PDC deposit in the Middleton area is variably welded, displaying a eutaxitic texture,
320 and is present only near Middleton Ridge (Fig. 7b). Fiamme of pumice and lithic clasts are
321 prevalent towards the base of the unit, with the degree of welding upwardly decreasing.
322 Towards the top of the unit, clasts of pumice, as well as lithic clasts of lava, oxidised lava and
323 cumulate fragments, are supported in a white ashy matrix, which is overlain by a pumice fall,
324 probably related to the same eruption. This unit is undated, but is older than ~ 600 ka.

325 Several thick pumice fall deposits are present within the central area of Ascension,
326 many of which are present within the stratigraphy on NASA Road and can be correlated to
327 closely surrounding areas (Fig. 5). Overlying a scoria fall deposit at the base of the Lower
328 NASA Road stratigraphy (Figs. 5 and 7c) is a 4 m thick, stratified pumice fall, containing a 6
329 cm ashy horizon rich in accretionary lapilli ('NASA Rd A'), and is dated at 667 ± 13 ka (AI14-
330 488B). Whole rock geochemical data suggests that this fall deposit may be zoned, with rhyolitic
331 compositions towards the base and trachytic pumice near the top (Table 3 and Fig. 6). The
332 pumice at the surface of NASA Rd A is yellow-coloured and weathered, suggesting a hiatus
333 before the next eruption. Overlying NASA Rd A, is a 10.4 m thick stratified pumice fall with
334 ashy layers ('NASA Road B') (Fig. 7c), which may correlate to a fall deposit on Upper NASA
335 Road dated at 664 ± 7 ka (AI16-708) (Fig 5).

336 The Goat Hole Ravine 1 ('GHR1') unit is of a similar age and is the oldest dated deposit
337 found in the east of Ascension. GHR1 is a > 14 m thick, stratified pumice lapilli (spL) situated
338 at the base of the Goat Hole Ravine sequence (605 ± 11 ka; AI15-630) (Figs. 8 and 9a). The
339 white trachyte (Table 3 and Fig. 6) pumice clasts often contain pink interiors, and some display

340 a brecciated texture, where fragmentation and annealing have occurred in the conduit. The
341 deposit contains abundant (up to ~ 40 %) lithic clasts, mainly comprising oxidised red scoria,
342 with lesser amounts of mafic lava and plutonic cumulate clasts. This unit has not been
343 correlated with any others on the island. In Goat Hole Ravine, it is unconformably overlain by
344 a breccia (pscBr) composed of pumice and scoria ('Pumice Scoria Breccia') (Fig. 8). Juvenile
345 clasts of pumice and scoria are generally < 10 cm in diameter, but scoria bombs up to ~ 50 cm
346 occur. Clasts of obsidian and plutonic cumulates also characterise this unit. This distinctive
347 unit correlates with deposits on Green Mountain Road, which have been dated at 634 ± 63 ka
348 (AI14-550). On Green Mountain Road, the 'Pumice Scoria Breccia' unit overlies Green
349 Mountain Road 1 in two locations (Fig. 2). On Green Mountain Road, the Pumice Scoria
350 Breccia is thicker (> 10 m) than in Goat Hole Ravine, and contains spatter-like scoria clasts,
351 indicating the eruption origin is probably more proximal to Green Mountain Road than Goat
352 Hole Ravine (Fig. 3c).

353 A distinctive unit in the central region is the 'Mingled Fall' deposit, which has been
354 described by Chamberlain et al. (2020), in relation to its geochemistry and melt inclusion
355 volatiles, which suggest rhyolite generation in the lower crust. This unit comprises a cm-thick
356 basal ash layer, overlain by mingled pumice clasts and gradually grades upwards to become
357 more scoria-dominated (Fig. 7d). This eruption unit occurs within the Lower NASA Road
358 sequence, and can be correlated to the hills around Upper NASA Road, Pyroclastic Plain,
359 Middleton Valley, and to the Green Mountain Road sequence (Fig. 5). The Mingled Fall
360 deposit is present in two places on Green Mountain Road, most notably on the Residency
361 Track, where it reaches its maximum thickness of 4 m and overlies the NASA PDC (Figs. 2
362 and 3b). Although it has not been directly dated, on Lower NASA Road it sits stratigraphically
363 between a pumice breccia dated at 693 ± 47 ka (AI14-491) and the NASA Road E pumice fall
364 (591 ± 17 ka; AI14-493A) (Fig. 7e).

365 NASA Road E pumice fall is the widest correlated unit in the central area of the island.
366 The thickest occurrence is on Lower NASA Road, where the fall deposit is ~ 35 m thick (Figs.
367 5 and 7e). It is one of the most prominent units on Green Mountain Road, where it is at least
368 20 m thick, although the top has been eroded and reworked (Figs. 2 and 3d). Based on field
369 characteristics, stratigraphic position and $^{40}\text{Ar}/^{39}\text{Ar}$ geochronology, it can also be correlated to
370 pumice lapilli deposits in Middleton Valley, Middleton Ridge, Two Boats, and the base of the
371 sequence inside Devil's Riding School (Fig. 5). The pumice lapilli is stratified (spL) and
372 interbedded with cm-thick, pink and yellow-coloured ashy layers. The whole rock SiO_2 content
373 decreases throughout the unit, with rhyolitic pumice near the base and trachytic pumice towards
374 the top (Table 3). As well as the sample from Lower NASA Road, which has been dated at 591
375 ± 17 ka (AI14-493A), the corresponding pumice on Green Mountain Road (AI16-714), as well
376 as the pumice fall at the base of the Devil's Riding School sequence (AI16-713) (Fig. 7f) have
377 also been dated, which are the same age within uncertainty as the main Lower NASA Road
378 deposit (Table 2). In comparison, Kar et al. (1998) obtained an age of 610 ± 20 ka for the
379 Devil's Riding School pumice, which is the same age, within uncertainty, as the age from this
380 study.

381 A noteworthy unit stratigraphically above NASA Road E in Devil's Riding School, is
382 the 'Devil's Eyeballs PDC' (Fig. 5). This unit comprises ~ 60 cm of cream-coloured ash with
383 matrix-supported lenses of pumice lapilli (mLT), overlain by an 80 cm bed of yellow-orange
384 ash and pumice lapilli containing very large (~ 3 cm diameter) concretions, known locally on
385 Ascension as 'devil's eyeballs' (Fig. 7g). The top of the unit is composed of creamy-yellow
386 ash, with lenses of pumice, probably reworked by water. This unit tentatively correlates with a
387 unit comprising several interbedded pumice lapilli and ash-rich lapilli tuff layers, situated on
388 Pyroclastic Plain (Fig. 7h), dated at 550 ± 23 ka (AI16-710) and is one of the youngest felsic

389 pyroclastic deposits in the central stratigraphy. Both occurrences are overlain by a 1 – 2 m
390 massive scoria fall (mscL) unit, of unknown origin.

391 In the east, there are multiple felsic pyroclastic deposits which erupted ~ 500 kyr ago.
392 This is particularly apparent in the area between Thistle Hill and Upper Valley Crater (Fig. 9b).
393 Here, 14 pumice units occur at the base of the stratigraphy, the majority of which erupted
394 around 500 kyr ago (Fig. 8, log 29). Within this sequence, most of the units are pyroclastic fall
395 units composed of trachytic or rhyolitic pumice lapilli (mpL, spL, dspL, bpL, fpL), with some
396 units containing horizons of tuff (mT, //sT), with evident bomb sag features in the lowermost
397 stratigraphic unit in this area (Fig. 8, log 29). Within the sequence, four units have been dated
398 at 549 ± 6 ka, 538 ± 14 ka, 505 ± 40 ka, 516 ± 12 ka (Fig. 8). In addition, the ‘North Green
399 Mountain’ pumice is present on the northern side of Green Mountain and in Upper Valley
400 Crater, dated at 530 ± 39 ka (AI14-508) (Fig. 8). This deposit comprises trachytic pumice lapilli
401 fall which is white, pink, or dark grey in colour, and some individual clasts display more highly
402 vesicular pink regions, and less vesicular dark grey portions. Above the pumice lapilli is a
403 horizon of welded and eutaxitic clasts interpreted to be a welded fall deposit (Fig. 9c). In Upper
404 Valley Crater, the pumice lapilli are overlain by an ashy layer rich in accretionary lapilli, which
405 grades up into the welded layer.

406

407 ***4.2 500-100 ka***

408 Notably, there are no dated pyroclastic units between ~ 500 and 100 ka, and few
409 pyroclastic deposits present within the stratigraphy which could have been emplaced during
410 this time period. There are four thin (< 1.3 m) pumice deposits near Thistle Hill which remain
411 undated, but stratigraphically overlie a pumice fall dated at 516 ± 12 ka (AI14-532) (Fig. 8 log
412 29). Based on the abundant deposits in this region which erupted in close succession (Fig. 8

413 log 29), it is probable that these deposits were emplaced close to ~ 500 ka. Based on the
414 stratigraphy, two prominent eruptions which did occur between 500 and 100 ka are the Green
415 Mountain Scoria and the Cricket Valley eruption.

416 The Green Mountain Scoria is present in the area between Thistle Hill and Upper Valley
417 Crater, as well as near the base of Cricket Valley, and near the summit of Green Mountain. The
418 summit of Green Mountain is composed of the eroded remnants of a scoria cone and represents
419 the proximal facies and vent region of the Green Mountain Scoria eruption. In Thistle Hill –
420 Upper Valley Crater and Cricket Valley, the deposit is a > 2 m thick, massive to stratified scoria
421 lapilli (mscL, sscL) fall unit, characterized by plutonic lithic clasts (Fig. 8). Associated with
422 this unit is a debris avalanche deposit, which occurs from the northern side of Green Mountain,
423 with the toe located at the aerial masts near Butt Crater (Figs. 1 and 9b). The debris avalanche
424 is composed of Green Mountain scoria, and directly overlies primary Green Mountain scoria
425 fall (Fig. 9d), so probably occurred close to the time of eruption. The boundary between
426 primary scoria fall and the base of the debris avalanche deposit can be defined by a ~ 3 cm
427 thick layer of finely ground and indurated (but not welded) scoria with slickensides.

428 Cricket Valley is an elongate crater with pyroclastic deposits around the edge. The
429 Green Mountain Scoria is deposited at the base of the sequence within Cricket Valley, overlain
430 by a ~ 1.5 m thick mafic lava flow, and the ‘Cricket Valley’ pyroclastic deposits (Fig. 8). The
431 ‘Cricket Valley pyroclastics’ have been previously described by Nielson and Sibbett (1996),
432 who recorded a thick sequence, with scoria lapilli at the base, overlain by a lithic explosion
433 breccia and then topped by laminated and cross bedded ash layers. We record a similar
434 sequence, comprising 16.5 m of red-orange coloured massive and stratified scoria lapilli and
435 ash, which is likely reworked towards the top. This is overlain by a 16 cm thick massive pumice
436 lapilli (mpL) fall unit, also recorded by Nielson and Sibbett (1996). Overlying this is a lithic
437 breccia (mlBr), containing blocks of mafic and trachytic lava, pumice, oxidised scoria, and

438 plutonic fragments. Bombs and bomb sag features are prevalent, with bombs up to ~ 1.5 m in
439 diameter (Fig. 9e). The lithic breccia is overlain by parallel- and cross-stratified ash (//sT, xsT)
440 layers, containing pumice lenses, likely deposited by dilute PDCs (surges) (Figs. 8 and 9f). In
441 total, the explosion breccia and surge layers are 25.5 m thick. Although the whole sequence
442 has previously been termed ‘Cricket Valley pyroclastics’ (Nielson and Sibbett, 1996), it is
443 likely to have formed via multiple eruptions, with the lithic breccia and surge layers potentially
444 associated with an eruption event which formed the current Cricket Valley crater. The pumice
445 fall present between the red-orange scoria and the lithic breccia likely originates from
446 elsewhere on the island, and although remains uncorrelated, it represents a time gap between
447 the emplacement of the scoria lapilli unit and the lithic breccia unit.

448

449 *4.3 < 100 ka*

450 There are multiple explosive eruptions which occurred ~ 100 ka, predominantly within
451 the eastern region of Ascension. The compositionally ‘Zoned Fall’ deposit is composed of
452 trachytic pumice lapilli at the base, gradually grading into basaltic trachy-andesite scoria lapilli
453 at the top of the unit (Chamberlain et al., 2016). This distinctive unit (Fig. 9g) is exposed in
454 Upper Valley Crater, the area between Upper Valley Crater and Thistle Hill, and at the NE
455 coast (e.g. Hummock Point, Echo Canyon). This unit is also found in more central localities
456 near Pyroclastic Plain and NASA Road, where it stratigraphically overlies the NASA Road
457 stratigraphy (Fig. 5 log 13). The unit thickens and coarsens towards the vent location, which is
458 a fissure located near the NE coast (Fig. 8 log 27 and Fig. 9h). This unit has been dated at 109
459 ± 12 ka (AI14-443) and is the only pumice unit as young as ~100 ka to be found in the central
460 region of the island. Another unit of a similar age, is the ‘Spire Beach’ eruption, dated at 106
461 ± 8 ka (AI14-434). This is a 28 m thick sequence of pumice lapilli and ash beds, with frequent

462 bomb sag features and lithic-rich (up to ~ 70% lithic clasts) horizons. This unit is not traced to
463 elsewhere on the island and represents the remnants of a tuff cone (Figs. 8 and 9i).

464 The youngest felsic pyroclastic deposits on Ascension Island occur in the east, with
465 several eruptions dated at ~ 60 ka. The trachytic 'Echo Canyon' eruption (59 ± 4 ka; AI15-
466 602A) (Fig. 4e,f) is often exposed stratigraphically above the Zoned Fall deposit (Fig. 8), and
467 is present along the NE coast (Fig. 9h) and near Spire Beach, with the thickest deposit located
468 within Echo Canyon. Within Echo Canyon, the sequence is ~ 50 m thick and broadly comprises
469 pumice lapilli beds (fall) at the base, overlain by a lapilli tuff with bomb sags, further pumice
470 lapilli, baked pink-orange pumice lapilli, and a layer of welded pumice fall (Fig. 9j). The
471 pumice clasts are variably vesiculated, comprising clasts of grey relatively low-density pumice
472 and green-grey micro-vesicular pumice (Fig. 9k). The pumice is characterised by the presence
473 of distinctive feldspar phenocrysts up to 3 – 4 mm in diameter, larger than in other pumice
474 deposits on Ascension. Along the NE coast, the Echo Canyon eruption is represented by
475 massive lapilli tuffs (ignimbrites), sometimes containing accretionary lapilli and beds of
476 pumice and lithic breccia. Within the 'Fissure Area' (Fig. 8 log. 27 and Fig. 9h), the Echo
477 Canyon pumice deposits appear in association with a lava dome and dome talus, which may
478 represent the later effusive stages of the Echo Canyon eruption.

479 The Echo Canyon eruption deposit is directly overlain by a thick felsic lava flow, the
480 'Ariane lava' flow (Fig. 1). Dating of this lava flow has been unsuccessful (29 ± 30 ka; AI14-
481 485), with the presence of excess argon ($^{40}\text{Ar}/^{36}\text{Ar} = 337$), and previous attempts have not
482 yielded sufficient argon to obtain an age (Nielson and Sibbett, 1996). Jicha et al. (2013)
483 obtained an age of 169 ± 43 ka, which is inconsistent with multiple ages in this study, although
484 the reason is not clear. Directly overlying the Ariane lava is the 'Devil's Cauldron' eruption
485 unit, dated at (64 ± 7 ka; AI14-509), implying close timing of the Echo Canyon, Ariane, and
486 Devil's Cauldron eruptions. The most complete, or key section of the 'Devil's Cauldron' unit

487 is exposed on top of the Ariane lava flow, where the unit is 16 m thick (Figs. 8 and 91). At the
488 base, the unit is ash-rich and dominantly composed of small (< 5 mm) angular clasts of trachyte
489 lava and abundant accretionary lapilli, with some pumice and clasts of obsidian. Pumice lapilli-
490 dominated beds gradually become prevalent at ~ 5m height from the base, with lithic clast
491 content ranging from ~10 – 30 %, comprising clasts of black and red oxidised mafic lava, and
492 obsidian. Clast-supported pumice lapilli layers are interbedded with ash-rich layers, containing
493 accretionary lapilli, bombs and bomb sag features. Towards the top of the deposit, rhyolitic
494 pumice has varying vesicularity, with both micro-vesicular and vesicular grey pumice clasts
495 present. The lithic clasts near the top of the deposit consist of black and red oxidised mafic
496 lava, trachyte lava, and plutonic fragments. To the west of this key section, the Devil's
497 Cauldron unit is present at the top of the Goat Hole Ravine sequence as interbedded layers of
498 accretionary lapilli and pumice lapilli. Further west, between Upper Valley Crater and Thistle
499 Hill, the corresponding deposits consist of 2 – 3 m of ash and accretionary lapilli. To the
500 southeast of the key section, near the Spire Beach Track (Fig. 8), the same unit contains ash
501 and abundant accretionary lapilli at the base, but is dominantly lithic-rich pumice and micro-
502 vesicular pumice lapilli, similar to the upper portions of the main deposit.

503

504 **5.0 Discussion**

505 *5.1 Felsic pyroclastic stratigraphy and correlations*

506 The preservation of the pyroclastic deposits on Ascension Island is variable. Many of
507 the units, especially older deposits, cannot be traced and often crop out in a single location,
508 uncorrelated to other localities. Even the most extensive units are restricted to small portions
509 of the island, correlated between few localities in close (max. ~ 3 – 4 km) proximity of each
510 other. The climate across Ascension varies, with persistent east-southeast trade winds resulting

511 in heavy precipitation in the southeast, and much drier conditions in the rain shadow of Green
512 Mountain, in the north and northwest of the island (Nielson et al., 1996). Rainfall tends to occur
513 as short periods of heavy precipitation, leading to flash floods and erosion (*e.g.* Rosenbaum,
514 1992). It is therefore probable that pyroclastic deposits have been subject to high rates of
515 erosion, due to heavy rainfall and flash flooding. The prevailing trade wind direction is evident
516 in the shape of scoria cones and scoria distribution, and it is likely that felsic pyroclastic
517 material would also be predominantly dispersed towards the northwest, with a portion
518 deposited in the ocean. Pyroclastic deposits may have been subsequently buried by lava flows
519 on the north and western flanks of the island, many of which are younger than the felsic
520 pyroclastic material (Jicha et al., 2013; Preece et al., 2018).

521 There are limited stratigraphic correlations between pyroclastic units deposited in the
522 central and eastern localities, with only the Zoned Fall deposit correlated between the two
523 regions. Pyroclastic units within the sequence on Green Mountain Road (Fig. 2) can be
524 correlated with some central and early eastern units. The ‘Mingled Fall, ‘NASA PDC’ and
525 ‘NASA Road E’ units can be correlated between the central localities and Green Mountain
526 Road, whereas the ‘Pumice Scoria Breccia’ crops out in the east and in the Green Mountain
527 Road sequence. In the central region of the island, evidence of vent location is limited, but
528 Devil’s Riding School, Green Mountain and Middleton Ridge are all probable vents for central
529 deposits. Within this region, individual pyroclastic eruptions have not been linked to a specific
530 vent location due to limited outcrop locations hindering the production of meaningful isopach
531 or isopleth maps. The vent localities for the older eastern deposits are not known, however they
532 may originate from the central region of the island. For example, units such as the ‘Pumice
533 Scoria Breccia’ and the ‘North Green Mountain’ appear to be more proximal closer to Green
534 Mountain. The younger eastern deposits can confidently be linked to eastern vent locations.
535 The ‘Zoned Fall’ originated from a fissure near the NE Coast (Fig. 9h), the ‘Spire Beach’ tuff

536 cone remnants are situated close to the vent, the ‘Echo Canyon’ eruption likely originated from
537 near the site of the Echo Canyon dome near the NE coast (Fig. 9h), and the ‘Devil’s Cauldron’
538 eruption probably erupted from Devil’s Cauldron crater. However, the preservation state, the
539 fact that deposits are proximal with any distal material deposited at sea, and the lack of definite
540 vent locations for the majority of eruptions, prohibits calculation of eruption volumes and
541 magnitudes.

542 In terms of their whole rock major element geochemistry (Table 3), pumice from this
543 study is mainly classed as trachyte and rhyolite, according to the total alkali-silica diagram (Le
544 Maitre, 1989) (Fig. 6). Generally, pumice > 500 ka has relatively lower alkali contents for a
545 given SiO₂ content compared to products < 100 ka, caused by a difference in Na₂O contents
546 (Fig. 6). However, this difference in alkali content is likely an alteration effect, with more Na₂O
547 loss in older samples compared to younger samples, rather than a change in magma chemistry
548 between eruptive periods. Although all samples were apparently fresh, many of the pumice
549 samples have high loss on ignition (LOI) values. Similar hydration is recorded in Ascension
550 pumice samples by whole rock major element and δ¹⁸O data, and is accompanied by Na₂O loss
551 when compared to lavas with similar SiO₂ contents (Weaver et al., 1996; Kar, 1997; Kar et al.,
552 1998). The majority of pumice samples in this study are apparently not sodic, and have a
553 peralkalinity index < 1, although this is also likely an artefact of Na loss during alteration (Table
554 3).

555

556 *5.2 Felsic explosive eruption chronology – timing and frequency*

557 The subaerial felsic pyroclastic record of Ascension Island spans nearly the last 1 Myr.
558 The oldest dated felsic pyroclastic unit is 916 ± 20 ka, found at the base of the Green Mountain
559 Road stratigraphy (GMR1 pumice fall). This is younger than the oldest subaerial felsic lava

560 flow age, previously dated at 1094 ± 12 ka (Jicha et al., 2013), although there could be further
561 pyroclastic units within the central region which are older, but remain undated due to their
562 weathered nature.

563 Taking into account stratigraphical and geochronological data, frequent explosive felsic
564 eruptions occurred from 916 ± 20 ka to approximately 500 ka. However, between
565 approximately 500 ka and 100 ka, there was an apparent hiatus in felsic pyroclastic activity.
566 There is a dearth of felsic explosive units emplaced during this time, with only the mafic Green
567 Mountain Scoria eruption, the Cricket Valley eruption, and four small, non-dated and non-
568 correlated pumice eruptions possibly occurring during this period (Fig. 8 logs 29 and 30). This
569 hiatus is particularly apparent in the stratigraphy of the region between Thistle Hill and Upper
570 Valley Crater (Fig. 8 logs 23 and 29). This hiatus can either be explained by the subsequent
571 removal of any felsic explosive deposits which may have been produced during this time
572 period, or alternatively, by a lack of felsic explosive eruptions during this time. The removal
573 of explosive products may, for example, be attributed to a large collapse event. However, there
574 are no deposits preserved on the island, or any geomorphological feature, which can be linked
575 to such a collapse. In addition, there is a lack of evolved lavas produced during this time, with
576 a predominance of basalt, hawaiiite and mugearite lavas erupted (Jicha et al., 2013). The lack
577 of felsic explosive and effusive products therefore suggests that the period of $\sim 500 - 100$ ka
578 was a predominantly mafic stage in the eruption history of Ascension. This is in general
579 agreement with the mafic volcanism phase proposed by Jicha et al. (2013) to have occurred
580 between 589 and 298 ka. This felsic hiatus may define the transition from activity of the Central
581 to the Eastern Felsic Complex. Between ~ 100 ka and 60 ka, at least 11 pumice-forming
582 explosive eruptions occurred on the east of the island, 7 of which have been dated. At
583 approximately 60 ka, the most-recent explosive felsic eruptions occurred. The Echo Canyon
584 (59 ± 4 ka) eruption, and the Devil's Cauldron eruption (64 ± 7 ka), separated by the Ariane

585 lava flow, all erupted near the NE coast within a short period of time, as the ages are
586 indistinguishable within the uncertainty of the $^{40}\text{Ar}/^{39}\text{Ar}$ measurements. Based on the $^{40}\text{Ar}/^{39}\text{Ar}$
587 uncertainties, taking into account the minimum age of the stratigraphically younger Devil's
588 Cauldron eruption and the maximum age of the stratigraphically older Echo Canyon eruption,
589 they erupted within a maximum time period of 6,000 years. Previously published felsic lava
590 ages from the east of the island are as young as 52 ± 3 ka (Jicha et al, 2013).

591 Based on the new data presented in this study, in conjunction with previously published
592 lava data from Jicha et al. (2013), four eruptive Periods are defined for the subaerial evolution
593 of Ascension (Fig. 10). Here, the term 'Period' is used to denote a volcanic activity unit,
594 characterised by products from eruptive centres over tens of thousands to millions of years.
595 Periods themselves may be part of a larger cycle, during which volcanic centres migrate and
596 geochemical differences may occur (Fisher and Schmincke, 1984; Lucchi, 2013). On
597 Ascension, Period 1 is the time period between ~ 1 Ma and 500 ka, defined from the earliest
598 dated exposed volcanic product (rhyolite lava flow dated at 1094 ± 12 ka; Jicha et al., 2013),
599 to the felsic hiatus. Throughout Period 1, felsic explosive and effusive eruptions occurred, with
600 mafic eruptions also evident within the geological record during this time. Activity during this
601 Period originated from the centre of the island, around Green Mountain, Middleton and Devils
602 Riding School, and therefore the felsic pyroclastics and lavas erupted during this Period are
603 associated with the Central Felsic Complex. Period 2 ($\sim 500 - 100$ ka) is characterised by a
604 scarcity of felsic products, and can be considered a mafic phase in the evolution of the island.
605 Period 3 consists of frequent felsic explosive and effusive eruptions which took place between
606 ~ 100 ka and 50 ka, with few mafic eruptions during this time. Field evidence points to vent
607 locations in eastern areas and therefore the felsic products of Period 3 are associated with the
608 Eastern Felsic Complex. During the time from the start of Period 3 until the most recent felsic
609 pyroclastic eruption (between approximately 100 ka and 60 ka), at least 11 explosive pumice-

610 forming eruptions occurred, with a mean reoccurrence interval of ~ 3.6 kyr. There is no record
611 of a felsic explosive eruption since ~ 60 ka, or a felsic lava flow younger than ~ 50 ka (Jicha et
612 al., 2013), with only mafic eruptions occurring since 50 ka. Given the felsic explosive
613 reoccurrence interval of ~ 3.6 kyr during Period 3, but a lack of any felsic eruption for the last
614 50 kyr (Fig. 10), the time since 50 ka may be denoted as a new Period (Period 4), dominated
615 by mafic eruptions, as young as 0.51 ± 0.18 ka (Preece et al., 2018).

616 Cyclic mafic and felsic periods are common features of ocean island volcanism. In
617 ocean islands settings, felsic melt generation is thought to be related to open-system fractional
618 crystallisation processes in the upper crust (< 5 km), with variable contribution from mafic
619 mixing and crustal assimilation (*e.g.* Jeffery and Gertisser, 2018 and references therein). At
620 other Atlantic islands, transitions between mafic and felsic periods can often be linked to
621 caldera formation. For example, Sete Cidades volcano, on São Miguel, Azores, has produced
622 several compositional cycles (Moore, 1991) linked to caldera formation, with post-caldera
623 activity associated with larger proportions of evolved material (*e.g.* Beier et al., 2006). On
624 Gough Island, basaltic volcanism ended with caldera formation, followed by volcanic
625 quiescence during which time fractional crystallisation processes produced subsequently
626 erupted trachytes (Le Maitre, 1960; Chevallier, 1987). On Tenerife, mafic injection into
627 shallow phonolitic reservoirs previously triggered caldera-formation, resulting in the
628 destruction of the shallow reservoir system (*e.g.* Triebold et al., 2006). After caldera collapse,
629 a 200 kyr mafic period ensued before phonolitic volcanism recommenced, which is thought to
630 be the time required to form new shallow evolved reservoirs capable of producing repeated
631 phonolitic eruptions (Marti and Gudmundsson, 2000). However, it is difficult to reconcile
632 processes responsible for mafic and felsic periods on other Atlantic islands with processes on
633 Ascension. On Ascension, there is no field evidence of a caldera, and there is evidence that at
634 least some felsic melts evolve via closed-system fractionation within the lower crust, at depths

635 of up to 11 km (Chamberlain et al., 2019; 2020). Potentially the magma reservoir(s) responsible
636 for formation of the Central Felsic Complex ceased being eruptible at ~ 500 ka. Mafic
637 magmatism continued for ~ 400 kyr, whilst new a felsic reservoir(s) assembled beneath the
638 east of the island, with the change in location perhaps induced by changes in the local stress
639 field (e.g. Marti and Gudmundsson, 2000). However, the reasons for this remain unclear and
640 warrant further petrological and geophysical investigation.

641

642 *5.3 Felsic explosive eruption styles and hazards*

643 The felsic pyroclastic deposits demonstrate that various eruptive styles have occurred
644 throughout the last 1 Myr of subaerial activity on Ascension, with evidence of both magmatic
645 and phreatomagmatic activity. The most common type of deposit associated with explosive
646 felsic eruptions on Ascension is pumice fall, as there are at least 73 pumice-bearing fall deposits
647 preserved on Ascension. Many of the pumice fall deposits are indicative of sustained eruption
648 columns, probably of subplinian scale. There are no prominent signs of caldera collapse on
649 Ascension which may be linked to a larger-scale eruption, although there are several lithic
650 breccia units, situated on Green Mountain Road and within the eastern areas. However, the
651 breccia units are localised, with no evidence of being linked to PDC deposits or caldera collapse
652 (e.g. lithic lag breccias), and are therefore more likely to be proximal explosion breccias.

653 Pyroclastic density current deposits on Ascension include pumice-rich ignimbrites,
654 welded eutaxitic PDC deposits, a dilute surge deposit, as well as scoria-bearing mafic PDC
655 deposits. In total, there is evidence in the stratigraphy for 16 PDC-forming eruptions, with some
656 PDC deposits associated with fall facies. For example, ignimbrites linked to the Echo Canyon
657 eruption, Devil's Eyeball's eruption, NASA PDC eruption, as well as the eutaxitic PDC deposits
658 found at Middleton, are all associated with fall facies produced during these eruptions. Other

659 PDC deposits are often discrete, weathered, matrix-supported and ash-rich units, not correlated
660 with any other unit. The PDCs formed during the Cricket Valley eruption are the only dilute
661 surge-type deposits on the island. Despite several lava domes situated in the east of Ascension,
662 there are no obvious block-and-ash flow deposits.

663 Phreatomagmatic deposits are found in the east of the island, including those of the
664 Spire Beach, Cricket Valley and Devils Cauldron eruptions. These deposits contain
665 characteristic phreatomagmatic features such as stratification of ash-rich and clast-rich layers,
666 accretionary lapilli, lithic clast-rich layers, cross-stratification and bomb sag features. In
667 addition, based on field characteristics, two other units near the base of the stratigraphy in the
668 Thistle Hill and Upper Valley Crater regions were likely formed via phreatomagmatic activity,
669 although have not been correlated elsewhere. These eruptions were subaerial, rather than
670 submarine phreatomagmatic eruptions, and therefore the water likely came into contact with
671 the magma via fractures and pores in the wall rock.

672 In summary, there are > 80 felsic explosive eruptions which erupted over the last 1 Myr,
673 evidenced within the subaerial stratigraphy. This should be regarded as a minimum estimate
674 due to erosion or burial of deposits, and the likelihood that much explosive material is deposited
675 at sea rather than on land.

676 The lack of felsic eruptions and predominance of mafic eruptions for the last 50 kyr,
677 raises questions about how any possible future eruption may proceed. The most recent
678 eruptions consisted of effusive and mild explosive activity, producing mafic lavas and scoria
679 in the NW of the island (Preece et al., 2018). Based on the most recent activity, it is likely that
680 future volcanic hazards may include lava flows, ballistics, tephra fallout and gas emissions
681 (Preece et al., 2018). However, given the abundance of felsic explosive deposits on the island
682 and previous cyclic activity, the possibility of another similar explosive eruption in the future
683 should not be ruled out. Recent textural observations from the Mingled Fall deposit, suggest

684 that magma can ascend rapidly, in timescales on the order of ~ 24 hours, emphasising the
685 importance of anticipating future activity on Ascension (Chamberlain et al., 2020). If a future
686 subplinian or phreatomagmatic eruption were to occur on Ascension, the entire island would
687 likely be affected by tephra fallout, topographically lower areas may be affected by PDCs, and
688 air travel could be disrupted, with the risk further compounded by Ascension's small size and
689 remote location.

690

691 **6.0 Conclusions**

692 Throughout the last 1 Myr, felsic eruptions have been commonplace on Ascension Island,
693 linked to a Central Felsic Complex and an Eastern Felsic Complex. Stratigraphic analysis,
694 $^{40}\text{Ar}/^{39}\text{Ar}$ geochronology and whole rock geochemical data reveal that between ~ 900 and 60
695 ka, more than 80 explosive felsic eruptions have occurred. Subplinian eruptions generated
696 pumice fall deposits up to ~ 40 m thick, welded fall deposits, ignimbrites and eutaxitic-textured
697 welded PDC deposits. In addition, phreatomagmatic eruptions can be associated with pumice
698 fall, massive lithic breccias, and dilute PDC (surge) deposits. Subaerial activity can be divided
699 into four eruption periods: Period 1 – felsic and mafic eruptions, with felsic explosive
700 eruptions, linked to the Central Felsic Complex (~ 1000 – 500 ka); Period 2 – mafic period
701 with dearth of felsic eruptions (~500 – 100 ka); Period 3 – felsic eruptions associated with the
702 Eastern Felsic Complex (100 – 50 ka); Period 4 – mafic eruptions. Although a felsic explosive
703 eruption hasn't occurred on Ascension for ~ 60 ka, and the most recent eruptions have consisted
704 of basaltic activity, a future explosive felsic eruption cannot be ruled out. These results reveal
705 the cyclical nature of Ascension Island volcanism and the timescales over which changes
706 between predominantly mafic and felsic volcanism occur, pertinent to better understanding
707 ocean island volcanism in general. This study highlights that frequent felsic explosive
708 eruptions, with wide-ranging styles, have taken place on Ascension Island throughout its

709 subaerial history, and therefore the possibility of a similar eruption occurring on Ascension in
710 the future remains possible.

711

712 **Acknowledgements**

713 We extend special thanks to the late Jon Davidson for dedication to the development and
714 progression of this project, and for stimulating and inspiring discussion. We thank the
715 Ascension Island Government and Conservation Department for permission to carry out the
716 work. Ascension Island Conservation Department, Ascension Island Heritage Society and
717 Drew Avery are thanked for logistical support during fieldwork. Thanks go to Ben Cohen,
718 Anna Hicks, Fin Stuart, Charlotte Vye-Brown and Barry Weaver for valuable discussions and
719 field assistance. We are grateful to Ross Dymock and Jim Imlach for assistance with $^{40}\text{Ar}/^{39}\text{Ar}$
720 sample preparation and technical support. Bertrand L  z   is acknowledged for technical
721 assistance with XRF analysis. This work was funded by a Leverhulme Trust Research Project
722 Grant (RPG-2013-042), with support from a Gloyne Outdoor Geological Research award from
723 the Geological Society of London. We thank reviewers Adriano Pimentel and Brian Jicha, for
724 their prompt reviews and constructive comments which helped to improve this manuscript, and
725 we thank Jose Luis Macias for Editorial handling.

726

727 **References**

- 728 Ammon, K., Dunai, T.J., Stuart, F.M., Meriaux, A.-S., Gayer, E. (2009) Cosmogenic ^3He
729 exposure ages and geochemistry of basalts from Ascension Island, Atlantic Ocean.
730 *Quaternary Geochronology*, 4, 525-532.
- 731 Atkins, F.B., Baker, P.E., Bell, J.D., Smith, D.G.W. (1964) Oxford expedition to Ascension
732 Island, 1964. *Nature*, 204, 722-724.

733 Beier, C., Haase, K.M., Hansteen, T.H. (2006) Magma evolution on Sete Cidades Volcano,
734 São Miguel, Azores. *Journal of Petrology*, 47, 1375-1411.

735 Bohrsen, W.A., Reid, M.R. (1997) Genesis of silicic peralkaline volcanic rocks in an ocean
736 island setting by crustal melting and open-system processes: Socorro Island, Mexico.
737 *Journal of Petrology*, 38, 1137-1166.

738 Branney, M.J., Kokelaar, P. (2002) Pyroclastic density currents and the sedimentation of
739 ignimbrites. *Geological Society of London, Memoir 27*, 152pp.

740 Brown, R.J., Branney, M.J. (2004) Event-stratigraphy of a caldera-forming ignimbrite eruption
741 on Tenerife: the 273 ka Poris Formation. *Bulletin of Volcanology*, 66, 392-416.

742 Brozena, J.M. (1986) Temporal and spatial variability of seafloor spreading processes in the
743 Northern South Atlantic. *Journal of Geophysical Research*, 91, 497-510.

744 Chamberlain, K.J., Barclay, J., Preece, K., Brown, R.J., Davidson, J.D., Edinburgh Ion
745 Microprobe Facility. (2016) Origin and evolution of silicic magmas at ocean islands:
746 perspectives from a zoned fall deposit on Ascension Island, South Atlantic. *Journal of*
747 *Volcanology and Geothermal Research*, 327, 349-360.

748 Chamberlain, K.J., Barclay, J., Preece, K., Brown, R.J., Davidson, J.D. (2019) Lower crustal
749 heterogeneity and fractional crystallisation control evolution of small-volume magma
750 batches at ocean island volcanoes (Ascension Island, South Atlantic). *Journal of*
751 *Petrology*, 60, 1489-1522.

752 Chamberlain, K.J., Barclay, J., Preece, K., Brown, R.J., McIntosh, I., Edinburgh Ion
753 Microprobe Facility. (2020) Deep and disturbed: conditions for formation and eruption
754 of a mingled rhyolite at Ascension Island, south Atlantic. *Volcanica*, 3, 139-153.

755 Chevellier, L. (1987) Tectonic and structural evolution of Gough Volcano: a volcanological
756 model. *Journal of Volcanology and Geothermal Research*, 33, 325-336.

757 Cousens, B.L., Clague, D.A., Sharp, W.D. (2003) Chronology, chemistry, and origin of
758 trachytes from Hualalai Volcano, Hawaii. *Geochemistry Geophysics Geosystems*, 4,
759 1078.

760 Daly, R.A. (1925) The geology of Ascension Island. *Proceedings of the American Academy*
761 *of Arts and Sciences*. 60, 1-80.

762 Darwin, C.R. (1844) Geological observations on the volcanic islands visited during the voyage
763 of H.M.S. Beagle, together with some brief notices of the geology of Australia and the
764 Cape of Good Hope. Being the second part of the geology of the voyage of the Beagle,
765 under the command of Capt. Fitzroy, R.N. during the years 1832 to 1836. London:
766 Smith Elder and Co.

767 Evangelidis, C.P., Minshull, T.A., Henstock, T.J. (2004) Three-dimensional crustal structure
768 of Ascension Island from active source tomography. *Geophysical Journal International*,
769 159, 311-325.

770 Fisher, R.V., Schmincke, H.-U. (1984) *Pyroclastic Rocks*. Springer-Verlag, Berlin, Heidelberg,
771 pp. 472.

772 Gertisser, R., Self, S., Gaspar, J.L., Kelley, S.P., Pimentel, A., Eikenberg, J., Barry, T.L.,
773 Pacheco, J.M., Queiroz, G., Vespa, M. (2010) Ignimbrite stratigraphy and chronology
774 on Terceira Island, Azores. In: Groppelli, G., Viereck-Goette, L. (Eds.) *Stratigraphy
775 and Geology of Volcanic Areas: Geological Society of America Special Paper 464*, p.
776 133–154

777 Guest, J.E., Gaspar, J.L., Cole, P.D., Queiroz, G., Duncan, A.M., Wallenstein, N., Ferreira, T.,
778 Pacheco, J.-M. (1999) Volcanic geology of Furnas Volcano, São Miguel, Azores.
779 *Journal of Volcanology and Geothermal Research*, 92, 1-29.

780 Harris, C., Bell, J.D., Atkins, F.B. (1982) Isotopic composition of lead and strontium in lava in
781 course-grained blocks from Ascension Island, South Atlantic. *Earth and Planetary
782 Science Letters*, 60, 79-85.

783 Harris, C. (1983) The petrology of lavas and associated plutonic inclusions of Ascension
784 Island. *Journal of Petrology*, 24, 424-470

785 Hobson, K. (2001) The pyroclastic deposits and eruption history of Ascension Island: a
786 palaeomagnetic and volcanological study. PhD Thesis, University of Oxford.

787 Jeffery, A.J., Gertisser, R. (2018) Peralkaline felsic magmatism of the Atlantic Islands.
788 *Frontiers in Earth Science*, 6:145.

789 Jicha, B.R., Singer, B.S. Valentine, M.J. (2013) $^{40}\text{Ar}/^{39}\text{Ar}$ geochronology of subaerial
790 Ascension Island and a re-evaluation of the temporal progression of basaltic to rhyolitic
791 volcanism. *Journal of Petrology*, 54, 2581-2596.

792 Jónasson, K. (2007) Silicic volcanism in Iceland: Composition and distribution within the
793 active volcanic zones. *Journal of Geodynamics*, 43, 101-117.

794 Kar, A. (1997) A comprehensive geological, geochemical, and petrogenetic study of hotspot-
795 related oceanic basaltic-rhyolite series rocks from Ascension Island, South Atlantic
796 Ocean. Unpublished PhD Thesis. University of Oklahoma, USA, 260pp.

797 Kar, A., Weaver, B., Davidson, J., Colucci, M. (1998) Origin of differentiated volcanic and
798 plutonic rocks from Ascension Island, South Atlantic Ocean. *Journal of Petrology*, 39,
799 1009-1024.

- 800 Klingelhöfer, F., Minshull, T.A., Blackman, D.K., Harben, P., Chilgers, V. (2001) Crustal
801 structure of Ascension Island from wide-angle seismic data: implications for the
802 formation of near-ridge volcanic islands. *Earth and Planetary Science Letters*, 190, 41-
803 56.
- 804 Kobberger, G., Schmincke, H.-U. (1999) Deposition of rheomorphic ignimbrite D (Mogán
805 Formation), Gran Canaria, Canary Islands, Spain. *Bulletin of Volcanology*, 60, 465-
806 485.
- 807 Komorowski, J.-C., Morin, J., Jenkins, S., Kelman, I. (2016) Challenges of volcanic crises on
808 Small Island States. In: Fearnley, C.J., Bird, D.K., Haynes, K., McGuire, W.J., Jolly,
809 G. (Eds.) *Observing the volcano world. Advances in Volcanology (An Official Book
810 Series of the International Association of Volcanology and Chemistry of the Earth's
811 Interior – IAVCEI, Barcelona, Spain)*. Springer, Cham.
- 812 Kuiper, K.F., Deino, A., Hilgen, F.J., Krijgsman, W., Renne, P.R., Wijbrans, J.R. (2008)
813 Synchronizing rock clocks of Earth history. *Science*, 320, 500-504.
- 814 Lee, J.Y., Marti, K., Severinghaus, J.P., Kawamura, K., Yoo, H.S., Lee, J.B., Kim, J.S. (2006)
815 A redetermination of the isotopic abundances of atmospheric argon. *Geochimica
816 Cosmochimica Acta*, 70, 4507-4512.
- 817 Legendre, C., Maury, R.C., Caroff, M., Guillou, H., Cotten, J., Chauvel, C., Bollinger, C.,
818 Hémond, C., Guille, G., Blais, S., Rossi, P., Savanier, D. (2005) Origin of exceptionally
819 abundant phonolites on Ua Pou Island (Marquesas, French Polynesia): partial melting
820 of basanites followed by crustal contamination. *Journal of Petrology*, 46, 1925-1962.
- 821 Le Maitre, R.W. (1960) The geology of Gough Island, South Atlantic. *Overseas Geology and
822 Mineral Resources*, 7, 1309-1340.
- 823 Le Maitre, R.W., Bateman, P., Dudek, A., Keller, J., Lameyre, J., Le Bas, M.J., Sabine, P.A.,
824 Schmid, R., Sorensen, H., Streckeisen, A., Woolley, A.R., Zanettin, B. (1989) *A
825 Classification of Igneous Rocks and Glossary of Terms: Recommendations of the
826 International Union of Geological Sciences Subcommission on the Systematics of
827 Igneous Rocks*. Oxford: Blackwell Scientific.
- 828 Lucchi, F., Tranne, C.A., Rossi, P.L. (2010) Stratigraphic approach to mapping of the late
829 Quaternary volcanic island of Lipari (Aeolian archipelago, southern Italy). In: Gropelli,
830 G., Viereck-Goette, L. (Eds.) *Stratigraphy and geology of volcanic areas: Geological
831 Society of America, Special Paper 464*, 1-32.
- 832 Lucchi, F. (2013) Stratigraphic methodology for the geological mapping of volcanic areas:
833 insights from the Aeolian archipelago (southern Italy). In: Lucchi, F., Peccerillo, A.,

834 Keller, J., Tranne, C.A., Rossi, P.L. (Eds.) The Aeolian Islands Volcanoes. Geological
835 Society, London, Memoirs, 37, 37-53.

836 Madeira, J., Mata, J., Mourão, C., Brum da Silveira, A., Martins, S., Ramalho, R., Hoffmann,
837 D.L. (2010) Volcano-stratigraphic and structural evolution of Brava Island (Cape
838 Verde) based on $^{40}\text{Ar}/^{39}\text{Ar}$, U-Th and field constraint. *Journal of Volcanology and*
839 *Geothermal Research*, 196, 219-235.

840 Mark, D.F., Barford, D., Stuart, F.M., Imlach, J. (2009) The ARGUS multicollector noble gas
841 mass spectrometer: Performance for $^{40}\text{Ar}/^{39}\text{Ar}$ geochronology: *Geochemistry*
842 *Geophysics Geosystems*, 10, Q0AA02.

843 Mark, D.F., Stuart, F.M., de Podesta, M. (2011) New high-precision measurements of the
844 isotopic composition of atmospheric argon. *Geochimica Cosmochimica Acta*, 75,
845 7494-7501.

846 Mark, D.F., Petraglia, M., Smith, V.C., Morgan, L.E., Barford, D.N., Ellis, B.S., Pearce, N.J.,
847 Pal, J.N., Korisettar, R. (2014) A high-precision $^{40}\text{Ar}/^{39}\text{Ar}$ age for the Young Toba Tuff
848 and dating of ultra-distal tephra: forcing of Quaternary climate and implications for
849 hominin occupation of India. *Quaternary Geochronology*, 21, 90-103.

850 Mark, D.F., Renne, P.R., Dymock, R.C., Smith, V.C., Simon, J.I., Morgan, L.E., Staff, R.A.,
851 Ellis, B.S., Pearce, N.J.G. (2017) High-precision $^{40}\text{Ar}/^{39}\text{Ar}$ dating of Pleistocene tuffs
852 and temporal anchoring of the Matuyama-Bruhnes boundary. *Quaternary*
853 *Geochronology*, 39, 1-23.

854 Marti, J., Gudmundsson, A. (2000) Las Cañadas caldera (Tenrife, Canary Islands): an
855 overlapping collapse caldera generated by magma-chamber migration. *Journal of*
856 *Volcanology and Geothermal Research*, 103, 161-173.

857 Marzocchi, W., Bebbington, M.S. (2012) Probabilistic eruption forecasting at short and long
858 time scales. *Bulletin of Volcanology*, 74, 1777-1805.

859 Minshull, T.A., Ishizuka, O., Garcia-Castellanos, D. (2010) Long-term growth and subsidence
860 of Ascension Island: constraints on the rheology of young oceanic lithosphere.
861 *Geophysical Research Letters*, 37, L23306.

862 Montelli, R., Nolet, G., Dahlen, F.A., Masters, G. (2006) A catalogue of deep mantle plumes:
863 New results from finite-frequency tomography. *Geochemistry, Geophysics,*
864 *Geosystems*, 7, Q11007.

865 Moore, R.B. (1991) Geology of three late Quaternary stratovolcanoes on São Miguel, Azores.
866 US Geological Survey Bulletin 1900, US Geological Service.

867 Murphy, M.A., Salvador, A. (1999) International Stratigraphic Guide – an abridged version.
868 International Subcommission on Stratigraphic Classification of IUGS International
869 Commission on Stratigraphy. *Episodes*, 22, 255-271.

870 Nielson, D. L., Sibbett, B.S. (1996) Geology of Ascension Island, South Atlantic Ocean.
871 *Geothermics*, 25, 427-448.

872 Nielson, D.L., Adams, M.C., Sibbett, B.S., Wright, P.M. (1996) Shallow thermal structure and
873 hydrology of Ascension Island, South Atlantic Ocean. *Geothermics*, 25, 521-541.

874 Niespolo, E., Rutte, D., Deino, A.L., Renne, P.R. (2017) Intercalibration and age of the Alder
875 Creek sanidine $^{40}\text{Ar}/^{39}\text{Ar}$ standard: Quaternary Geochronology, 39, 205-213.

876 Paulick, H., Münker, C., Schuth, S. (2010) The influence of small-scale mantle heterogeneities
877 on Mid-Ocean Ridge volcanism: Evidence from the southern Mid-Atlantic Ridge
878 ($7^{\circ}30'S$ to $11^{\circ}30'S$) and Ascension Island. *Earth and Planetary Science Letters*, 296,
879 299-310.

880 Pickersgill, A.E, Mark, D.F, Lee, M.R., Osinski, G.R. (2020) $^{40}\text{Ar}/^{39}\text{Ar}$ systematics of melt
881 lithologies and target rocks from the Gow Lake impact structure, Canada. *Geochimica
882 et Cosmochimica Acta*, 274, 317-332.

883 Pimentel, A., Pacheco, J., Self, S. (2015) The ~1000 years BP explosive eruption of Caldeira
884 Volcano (Faial, Azores): the first stage of incremental caldera formation. *Bulletin of
885 Volcanology*, 77, 42.

886 Preece, K., Mark, D.F., Barclay, J., Cohen, B.E., Chamberlain, K.J., Jowitt, C., Vye-Brown,
887 C., Brown, R.J., Hamilton, S. (2018) Bridging the gap: $^{40}\text{Ar}/^{39}\text{Ar}$ dating of volcanic
888 eruptions from the ‘Age of Discovery’, *Geology*, 46, 1035-1038.

889 Queiroz, G., Pacheco, J.M., Gaspar, J.L., Aspinall, W.P., Guest, J.E., Ferreira, T. (2008) The
890 last 5000 years of activity at Sete Cidades volcano (São Miguel Island, Azores):
891 implications for hazard assessment. *Journal of Volcanology and Geothermal Research*,
892 178, 562-573.

893 Renne, P.R. (2014) Some footnotes to the optimization-based calibration of the $^{40}\text{Ar}/^{39}\text{Ar}$
894 system. *Geological Society of London Special Publication*, 378, 21-31.

895 Renne, P.R., Norman, E.B. (2001) Determination of the half-life of ^{37}Ar by mass spectrometry.
896 *Physical Review C*, 63, 047302.

897 Renne, P.R., Sharp, Z.D., Heizler, M.T. (2008) Cl-derived argon isotope production in the
898 CLICIT facility of OSTR reactor and effects of the Cl-correction in $^{40}\text{Ar}/^{39}\text{Ar}$
899 geochronology. *Chemical Geology*, 255, 463-466.

900 Renne, P.R., Cassata, W.S., Morgan, L.E. (2009) The isotopic composition of atmospheric
901 argon and $^{40}\text{Ar}/^{39}\text{Ar}$ geochronology: time for a change? *Quaternary Geochronology*, 4,
902 288-298.

903 Renne, P.R., Mundil, R., Balco, G., Min, K., Ludwig, K.R. (2010) Joint determination of ^{40}K
904 decay constants and $^{40}\text{Ar}^*/^{40}\text{K}$ for the Fish Canyon sanidine standard, and improved
905 accuracy for $^{40}\text{Ar}/^{39}\text{Ar}$ geochronology. *Geochimica Cosmochimica Acta*, 74, 5349-
906 5367.

907 Renne, P.R., Mundil, R., Balco, G., Min, K., Ludwig, K.R. (2011) Response to comment by
908 W. H. Schwarz et al. on “Joint determination of ^{40}K decay constants and $^{40}\text{Ar}^*/^{40}\text{K}$ for
909 the Fish Canyon sanidine standard, and improved accuracy for $^{40}\text{Ar}/^{39}\text{Ar}$
910 geochronology”. *Geochimica Cosmochimica Acta*, 75, 5097-5100.

911 Rosenbaum, M.S. (1992) The geology of Ascension Island. *Geology Today*, 8, 180-184.

912 Selva, J., Acocella, V., Bisson, M., Caliro, S., Costa, A., Della Seta, M., De Martino, P., de
913 Vita, S., Frederico, C., Giordano, G., Martino, S., Cardaci, C. (2019) Multiple natural
914 hazards at volcanic islands: a review for the Ischia volcano, Italy. *Journal of Applied*
915 *Volcanology* 8:5.

916 Shea, T., Owen, J. (2016) Discovery of a trachyte ignimbrite sequence at Hualālai, Hawaii.
917 *Bulletin of Volcanology*, 78, 34.

918 Stoenner, R.W., Oa, S., Katcoff, S. (1965) Half-lives of Argon-37, Argon-39 and Argon-42.
919 *Science*, 148, 1325.

920 Triebold, S., Kronz, A., Wörner, G. (2006) Anorthite-calibrated backscattered electron
921 profiles, trace elements, and growth textures in feldspars from the Teide-Pico Viejo
922 volcanic complex. *Journal of Volcanology and Geothermal Research*, 154, 117-130.

923 van den Bogaard, P. (1998) $^{40}\text{Ar}/^{39}\text{Ar}$ ages of Pliocene-Pleistocene fallout tephra layers and
924 volcanoclastic deposits in the sedimentary aprons of Gran Canaria and Tenerife (Sites
925 953, 954 and 956). *Proceedings of the Ocean Drilling Program, Scientific Results*, 157,
926 329-341.

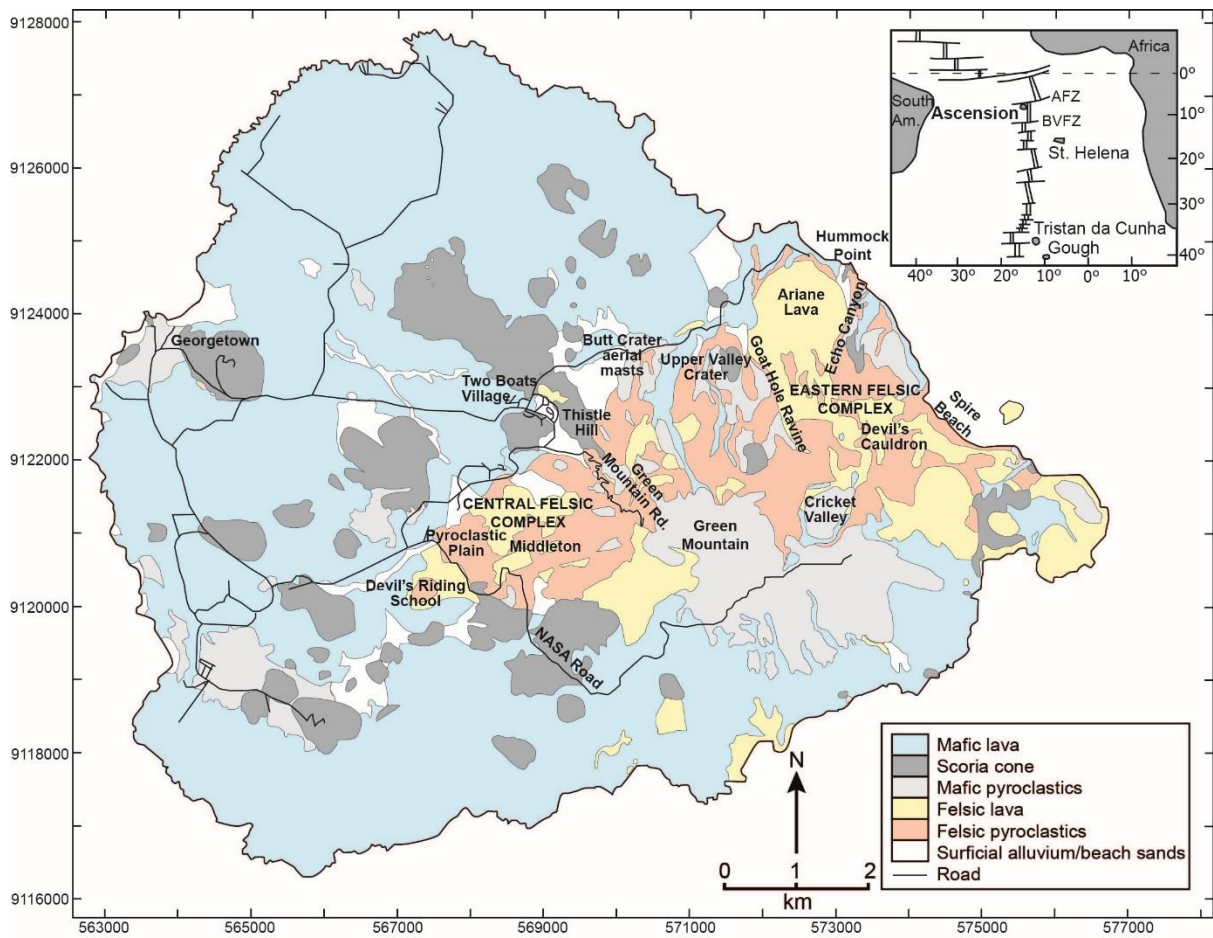
927 Weaver, B., Kar, A., Davidson, J., Colucci, M. (1996) Geochemical characteristics of volcanic
928 rocks from Ascension Island, South Atlantic Ocean. *Geothermics*, 25, 449-470.

929 Wilkinson, E., Lovell, E., Carby, B., Barclay, J., Robertson, R.E.A. (2016) The dilemmas of
930 risk-sensitive development on a small volcanic island. *Resources*, 5, 21.

931

932

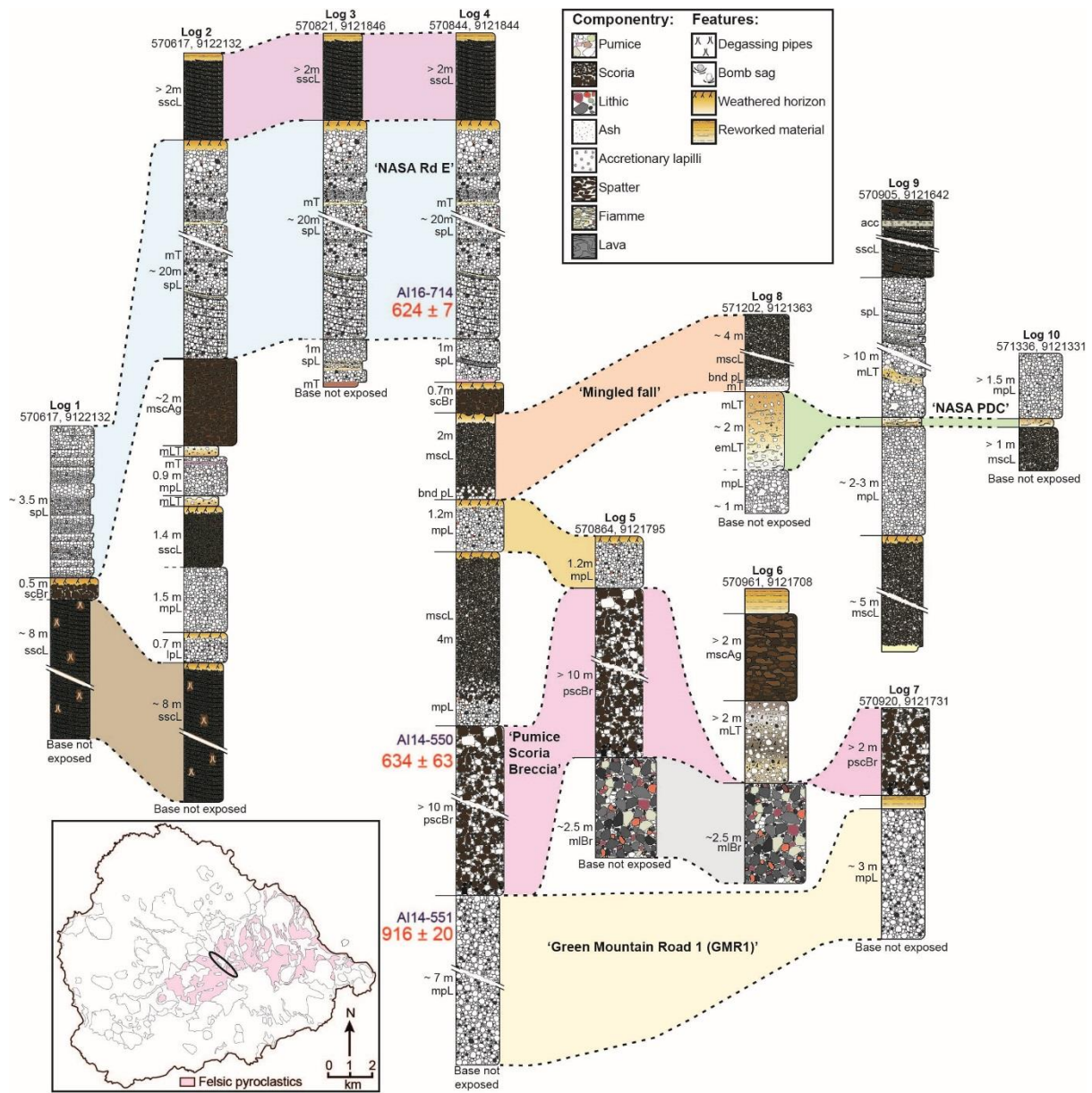
934



935

936 **Fig 1:** Geological map of Ascension Island (modified after Nielson and Sibbett, 1996), showing
937 roads, settlements and localities referred to in this work. Inset: location map of Ascension at
938 the southern Mid-Atlantic Ridge, between the Ascension Fracture Zone (AFZ) and the Bode
939 Verde Fracture Zone (BVFZ) (modified after Paulick et al., 2010).

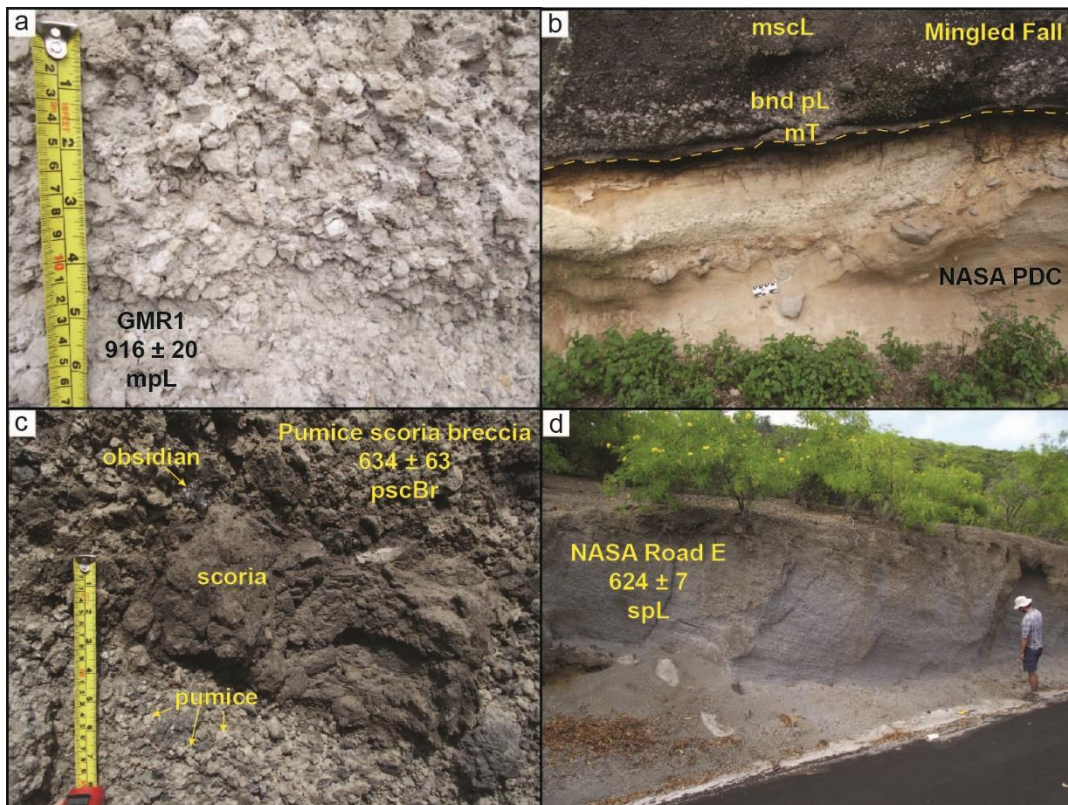
940



941

942 **Fig 2:** Stratigraphic logs of the pyroclastic products situated on Green Mountain Road. Each
 943 unit is labelled with the lithofacies present. Sample numbers are shown for units where XRF
 944 and/or $^{40}\text{Ar}/^{39}\text{Ar}$ data has been collected, and $^{40}\text{Ar}/^{39}\text{Ar}$ ages (in ka \pm 2-sigma analytical
 945 uncertainty) are shown.

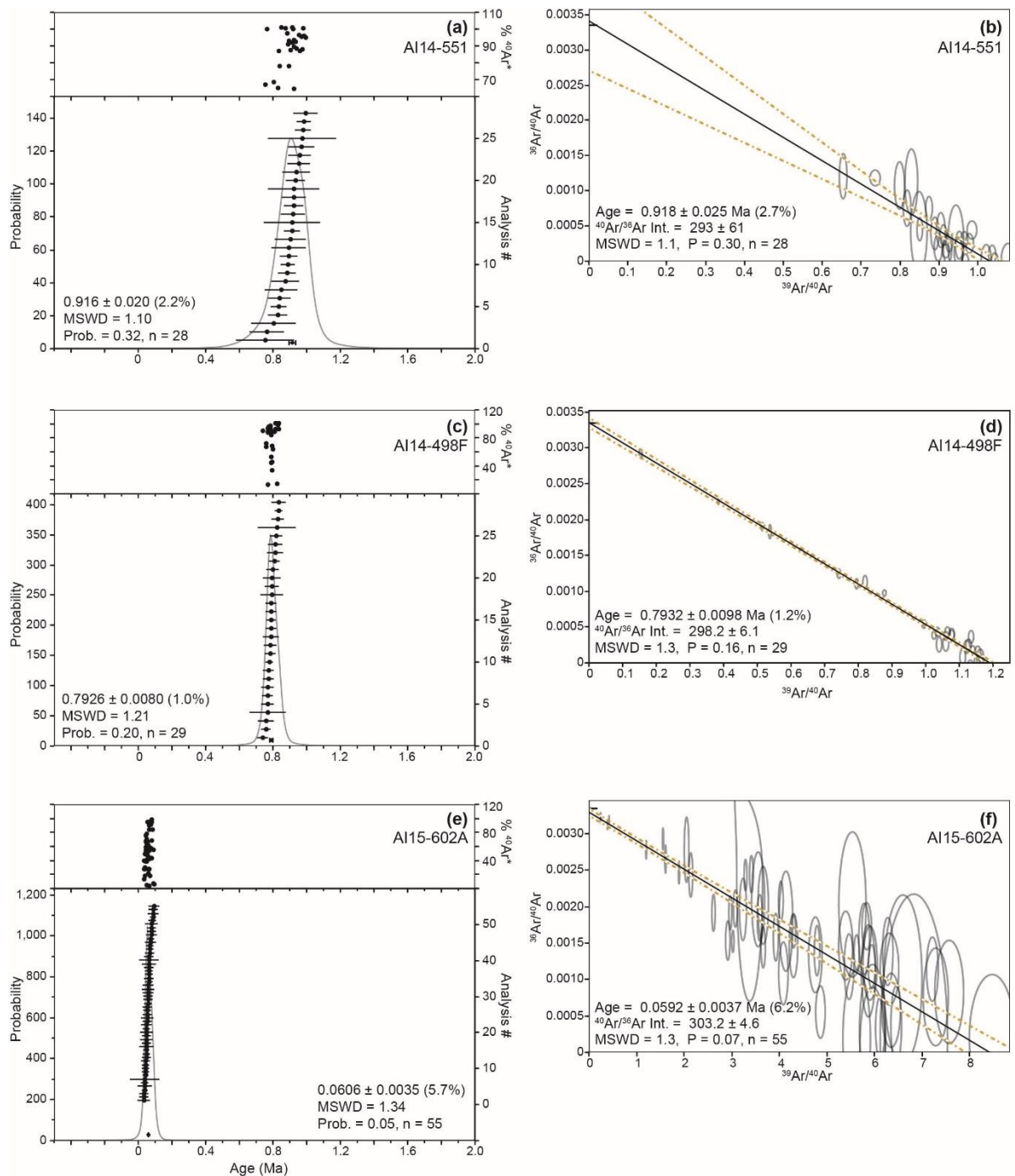
946



947

948 **Fig 3:** Photographs of Green Mountain Road pyroclastic deposits, showing eruptive units,
 949 lithofacies, and $^{40}\text{Ar}/^{39}\text{Ar}$ ages (in ka \pm 2-sigma analytical uncertainty) where relevant: a)
 950 GMR1 pumice fall deposit; b) the Mingled Fall unit overlying the NASA PDC deposit on the
 951 Residency Track; c) Pumice Scoria Breccia unit, with bombs of scoria, pumice clasts and
 952 obsidian clasts; d) part of the NASA Road E unit on Green Mountain Road.

953

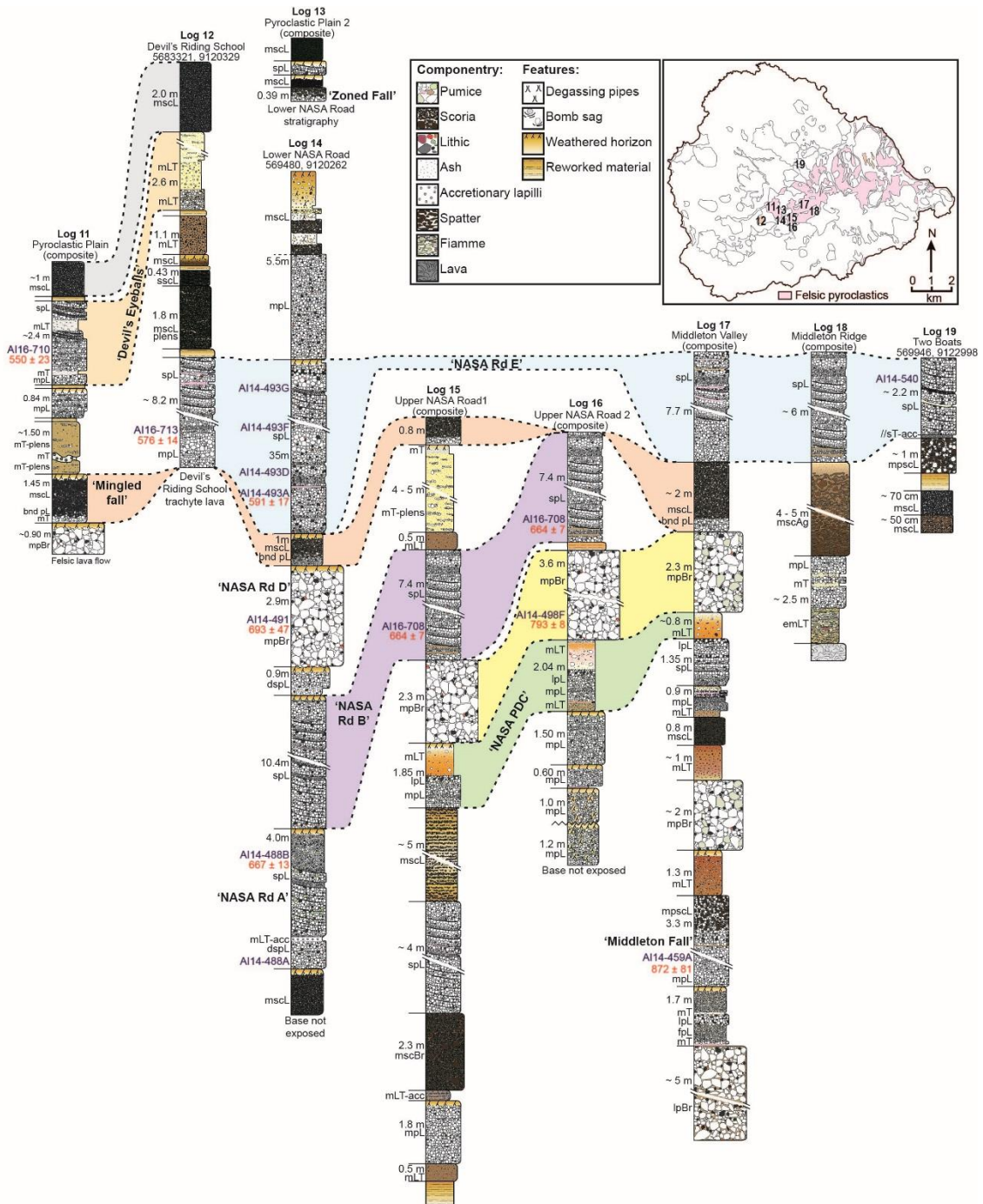


954

955 **Fig. 4:** Example ⁴⁰Ar/³⁹Ar age probability spectra and inverse isochrons. The ages calculated
 956 with each method are indistinguishable from each other for all samples: a) age probability
 957 spectra for AI14-551 GMR1; b) inverse isochron for AI14-551 GMR1; c) age probability
 958 spectra for AI14-498F Upper NASA Road pumice breccia; d) inverse isochron for AI14-498F
 959 Upper NASA Road pumice breccia; e, f) age probability spectra and inverse isochron for AI15-
 960 602A Echo Canyon eruption. This is an example where the ⁴⁰Ar/³⁶Ar is distinguishable from

961 atmosphere and therefore the inverse isochron age is more appropriate. See Supplementary
 962 Material for all age probability spectra and inverse isochrons and for $^{40}\text{Ar}/^{39}\text{Ar}$ data.

963

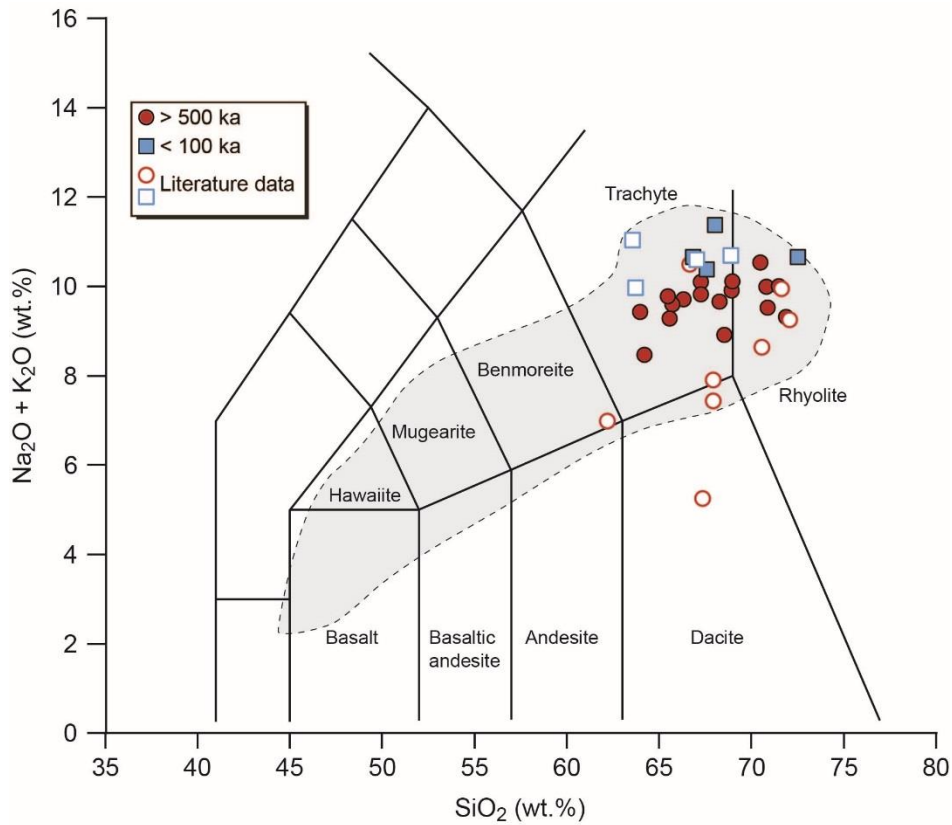


964

965 **Fig 5:** Stratigraphic logs of the pyroclastic products located within the central region of
 966 Ascension. Each unit is labelled with the lithofacies present. Sample numbers are shown for

967 units where XRF and/or $^{40}\text{Ar}/^{39}\text{Ar}$ data has been collected, and $^{40}\text{Ar}/^{39}\text{Ar}$ ages (in ka \pm 2-sigma
968 analytical uncertainty) are shown.

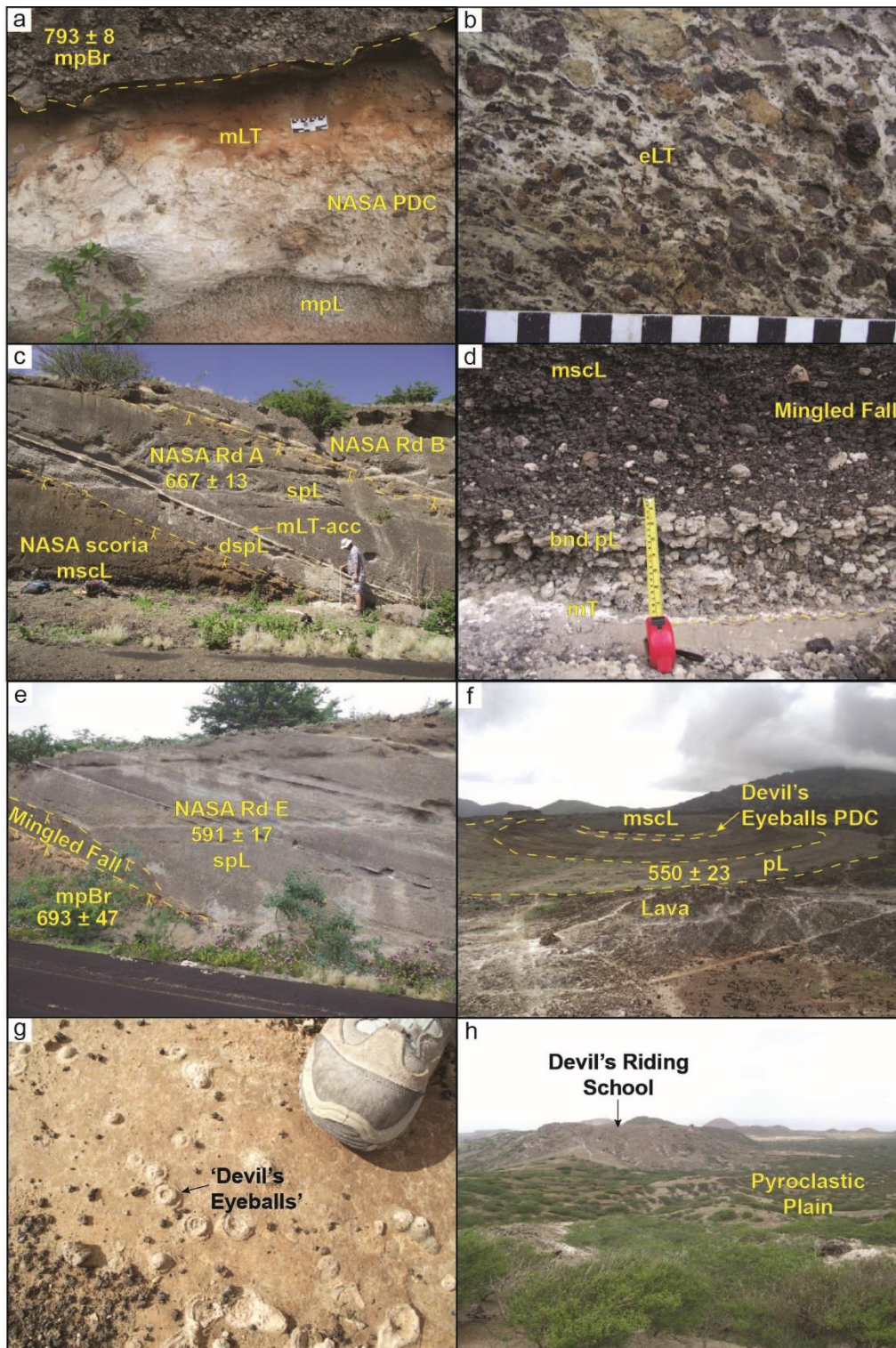
969



970

971 **Fig. 6:** Total alkali vs. SiO₂ diagram of pumice samples > 500 ka and < 100 ka. Literature
972 pumice XRF data taken from Weaver et al. (1996); Kar et al. (1998); Chamberlain et al. (2016,
973 2019, 2020). Grey field defines published Ascension XRF data, including lavas and scoria with
974 data from Weaver et al. (1996); Kar et al. (1998); Ammon et al. (2009); Jicha et al. (2013);
975 Chamberlain et al. (2019). All values normalised to 100 wt. % on a volatile-free basis.

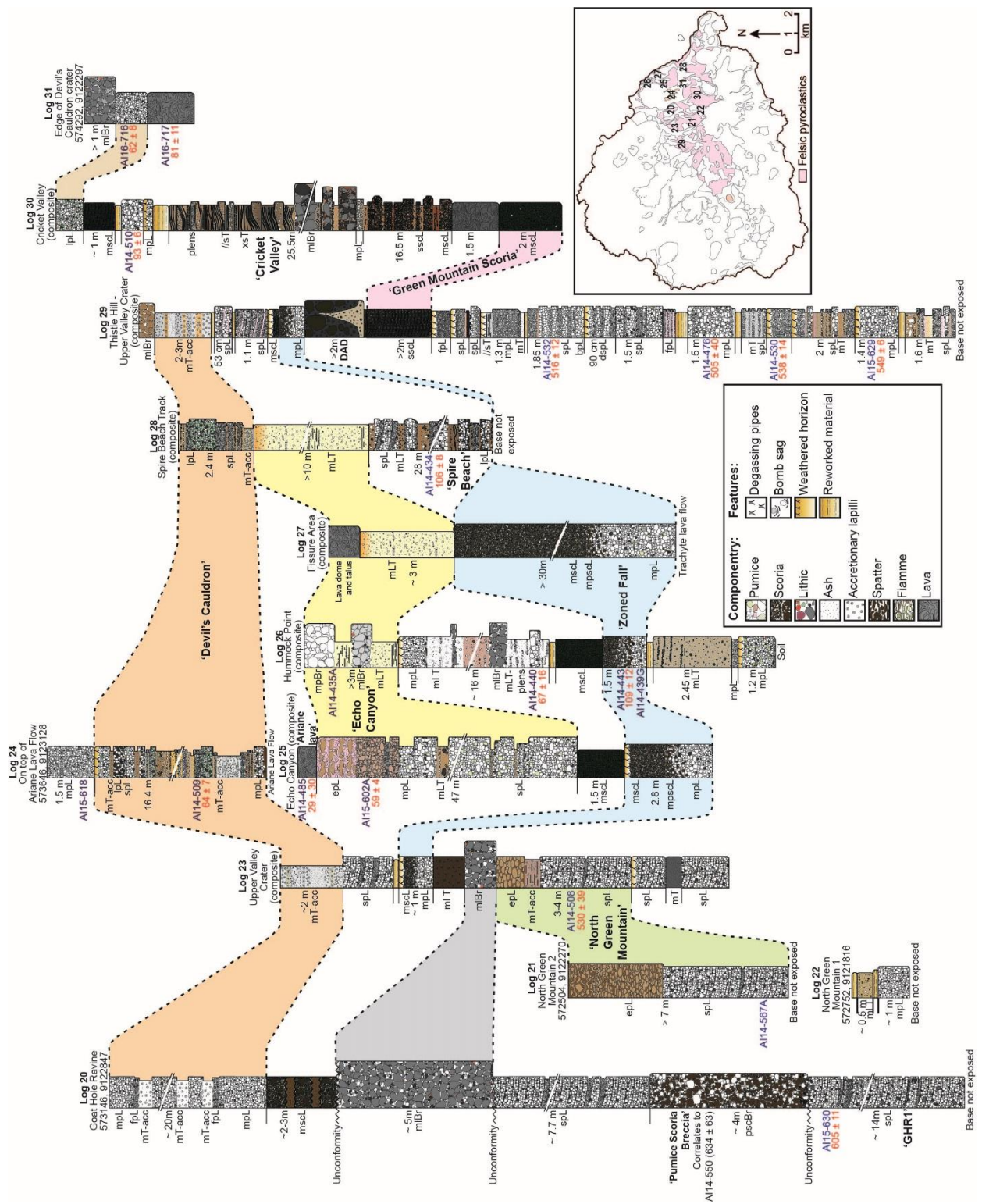
976



977

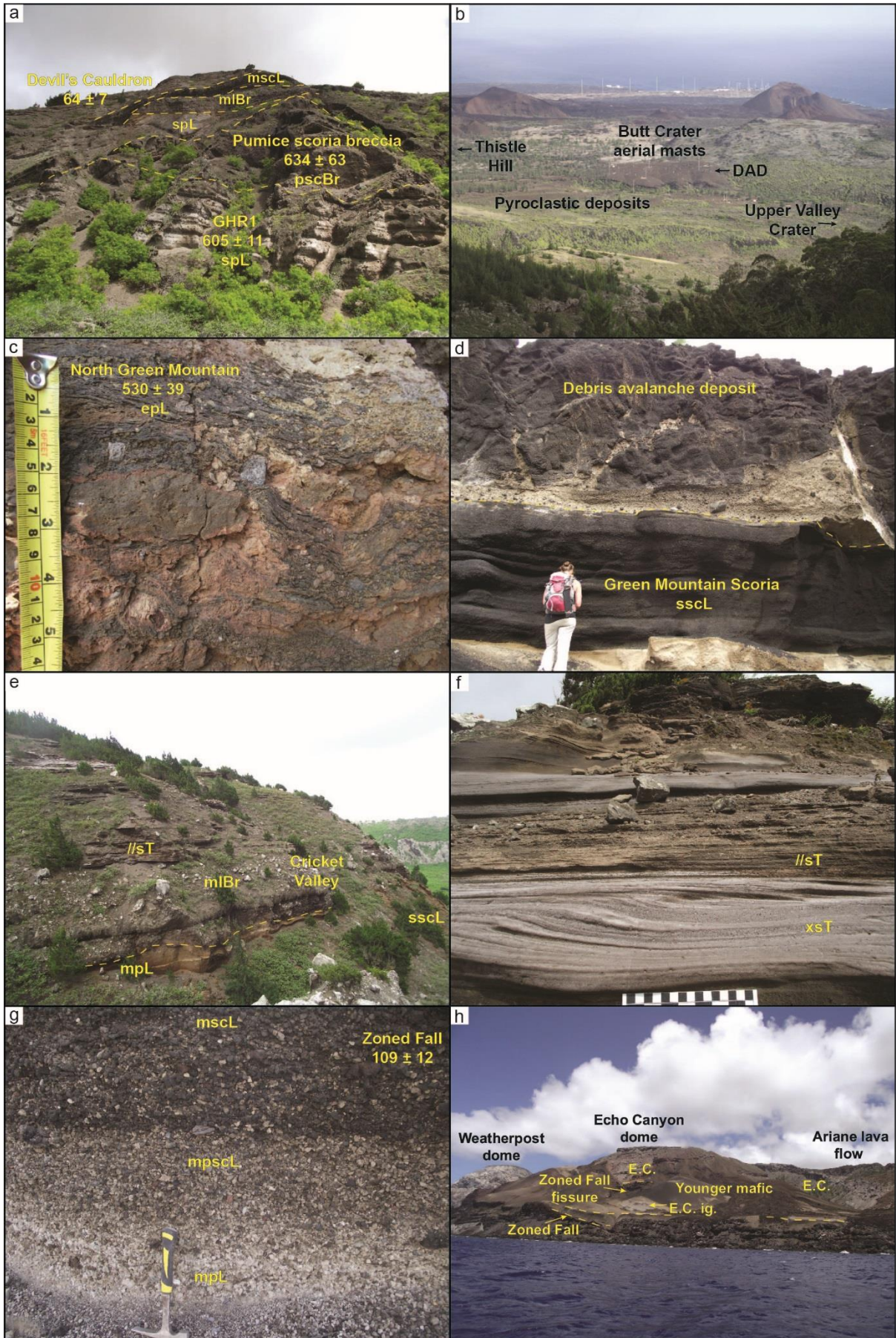
978 **Fig 7:** Photographs of pyroclastic deposits located in the centre of Ascension, showing eruptive
 979 units, lithofacies, and $^{40}\text{Ar}/^{39}\text{Ar}$ ages where relevant: a) NASA ignimbrite and overlying
 980 pumice breccia situated on Upper NASA Rd; b) eutaxitic, variably welded PDC deposit located
 981 near Middleton Ridge; c) Lower NASA Rd sequence – Lower NASA A and B; d) the Mingled

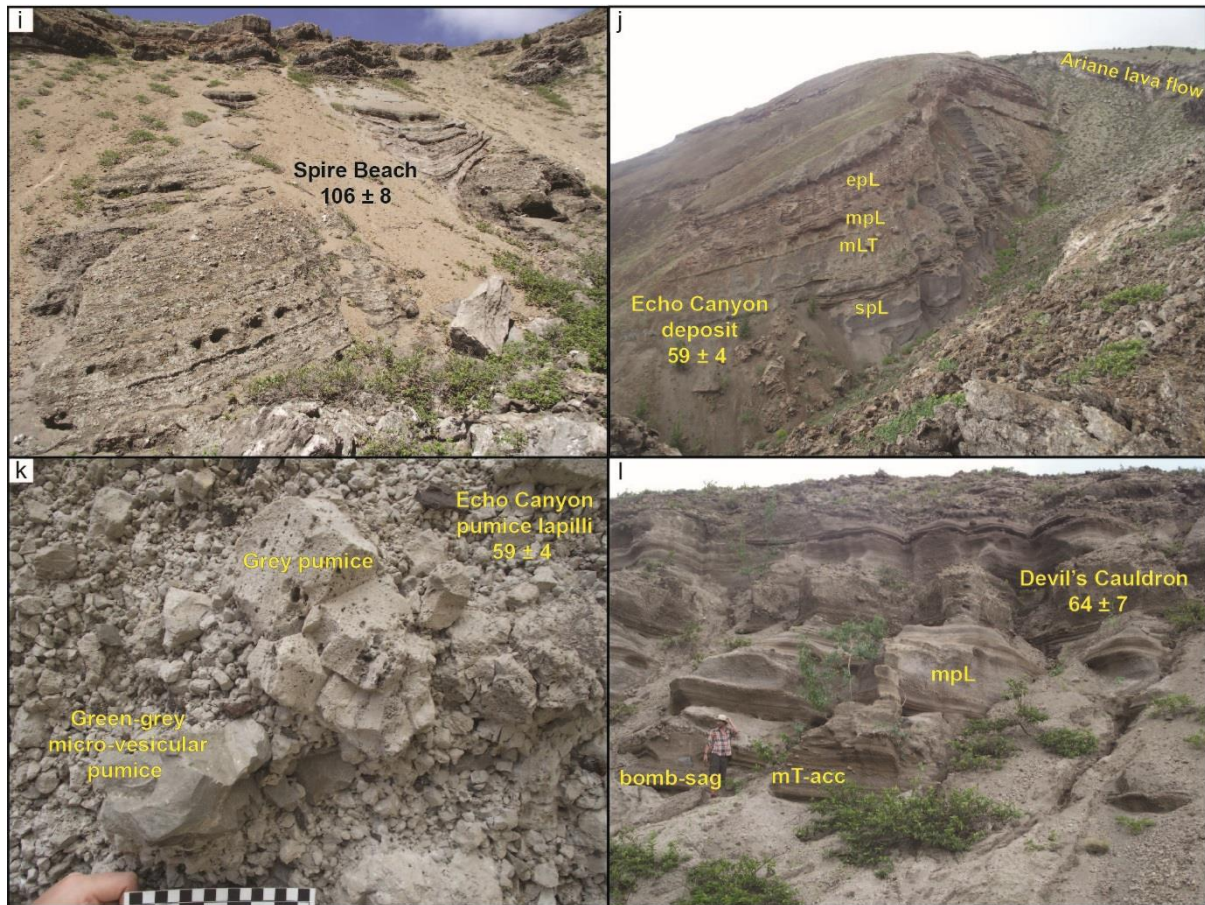
982 Fall deposit on Pyroclastic Plain; e) Lower NASA Rd sequence – massive pumice breccia,
983 Mingled Fall and NASA Rd E; f) overview of Devil’s Riding School - a crater filled with
984 pyroclastic deposits subsequently eroded to reveal a concentric, inwardly-dipping sequence;
985 g) a view over Pyroclastic Plain and Devil’s Riding School, as seen from Lower NASA Road.
986



987

988 **Fig 8:** Stratigraphic logs of the pyroclastic products located in the east of the island. Each unit
 989 is labelled with the lithofacies present. Sample numbers are shown for units where XRF and/or
 990 ⁴⁰Ar/³⁹Ar data has been collected, and ⁴⁰Ar/³⁹Ar ages (in ka ± 2-sigma analytical uncertainty)
 991 are shown.





993

994 **Fig 9:** Photographs of pyroclastic deposits situated in the east of Ascension, showing eruptive

995 units, lithofacies, and $^{40}\text{Ar}/^{39}\text{Ar}$ ages (in ka \pm 2-sigma analytical uncertainty) where relevant:

996 a) overview of Goat Hole Ravine section; b) overview of area between Thistle Hill (out of
 997 frame) and Upper Valley Crater, viewed from Green Mountain looking towards the northwest.

998 The area is the site of many pyroclastic deposits and the debris avalanche deposit (DAD); c)
 999 eutaxitic welded fall forming the top of the North Green Mountain unit exposed in a location

1000 on the northern side of Green Mountain; d) Green Mountain Scoria unit and overlying debris

1001 avalanche deposit composed of the same scoria; e) Cricket Valley eruption deposit showing

1002 massive lithic breccia (mlBr) overlain by stratified (//sT) surge deposits; f) cross- and parallel-

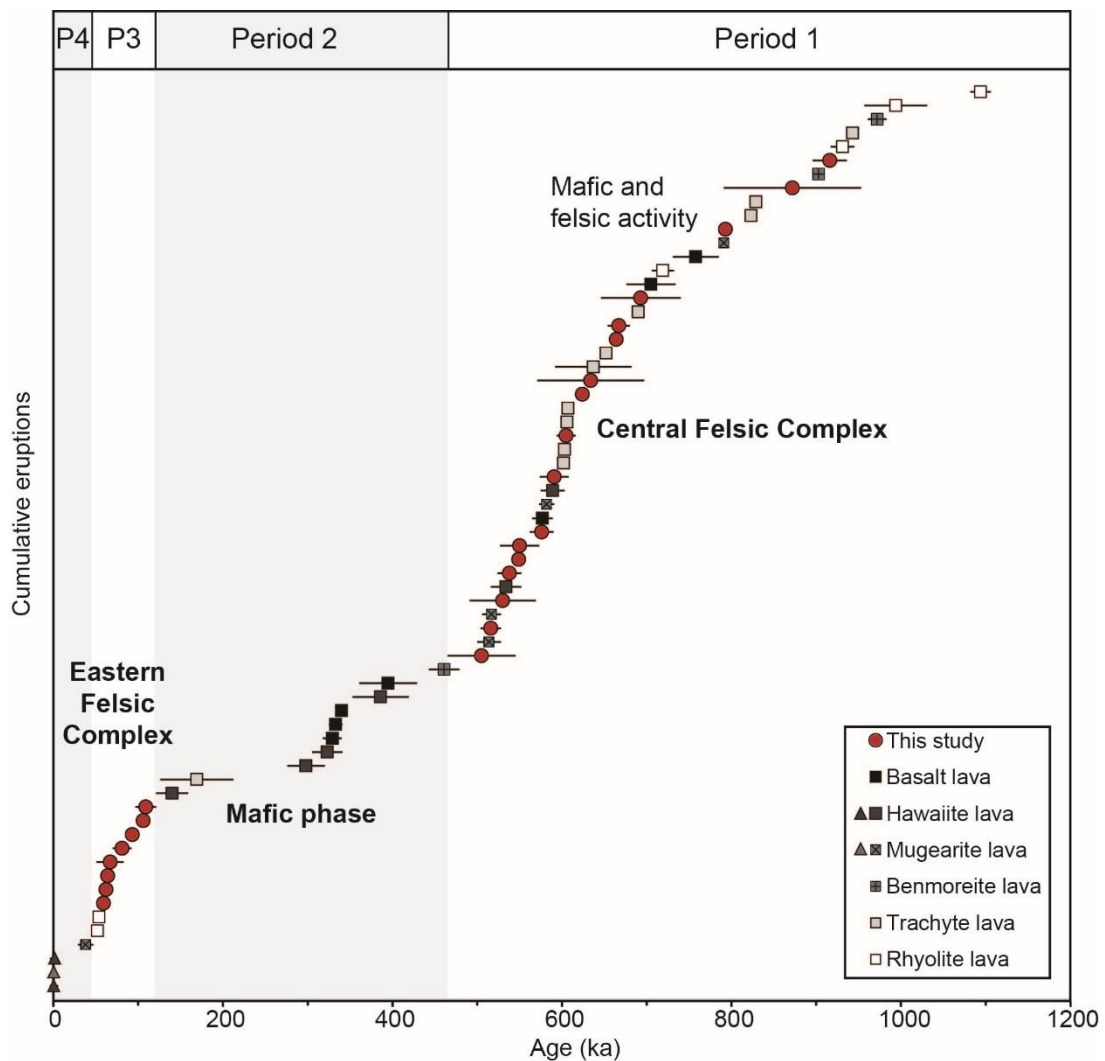
1003 stratified tuff (xsT, //sT) deposited by dilute PDCs (surges) during the Cricket Valley eruption;

1004 g) the Zoned Fall deposit; h) part of the northeast coast, southeast of Hummock Point, viewed

1005 from offshore. The Zoned Fall and its associated fissure region is overlain by the Echo Canyon

1006 (E.C.) eruption deposits (ignimbrite facies and dome), overlain by the Ariane Flow and mafic
 1007 deposits; i) the Spire Beach tuff cone deposits; j) an overview of Echo Canyon and the Echo
 1008 Canyon eruption deposits, overlain by the Ariane lava flow; k) Echo Canyon pumice fall
 1009 showing clasts with different vesicularity; l) overview of the Devil's Cauldron unit situated on
 1010 top of the Ariane lava flow.

1011



1012

1013 **Fig. 10:** $^{40}\text{Ar}/^{39}\text{Ar}$ ages (2σ uncertainty) for all pumice eruptions in this study, with additional
 1014 lava ages and compositions from Jicha et al., (2013) (squares) and Preece et al. (2018)
 1015 (triangles). The subaerial eruptive history may be divided into four eruptive periods based on
 1016 these ages and the stratigraphy. See text for further explanation.